A mitochondrial stress-specific form of HSF1

protects against age-related proteostasis collapse

Rhianna Williams, Mihails Laskovs, Rebecca I. Williams, Ananya Mahadevan and John Labbadia[1*]

[1] Institute of Healthy Ageing; Dept of Genetics, Evolution and Environment, University College London, Darwin Building, Gower Street, London, WC1E 6BT

*****corresponding and lead author: j.labbadia@ucl.ac.uk

Summary

The loss of protein homeostasis (proteostasis) is a primary driver of age-related tissue dysfunction. Recent studies have revealed that the failure of proteostasis with age is triggered by developmental and reproductive cues that repress the activity of proteostasis-related pathways in early adulthood. In *Caenorhabditis elegans*, reduced mitochondrial electron transport chain (ETC) function during development can override signals that promote proteostasis collapse in aged tissues. However, it is unclear precisely how these beneficial effects are mediated. Here, we reveal that in response to ETC impairment, the PP2A complex generates a dephosphorylated, mitochondrial stress-specific variant of the transcription factor HSF-1. This results in the selective induction of small heat shock proteins in adulthood, thereby protecting against age-related proteostasis collapse. We propose that mitochondrial signals early in life can protect the ageing cytosolic proteome by tailoring HSF-1 activity to preferentially drive the expression of non-ATP dependent chaperones.

Keywords: proteostasis, protein aggregation, molecular chaperones, HSF1, mitochondria, stress responses, ageing, PP2A, reactive oxygen species,

Introduction

Among the many hallmarks of ageing, the loss of protein homeostasis (proteostasis) is considered to be a primary driver of age-associated tissue dysfunction (Lopez-Otin et al., 2013). Proteostasis is maintained through the action of the proteostasis network (PN), a collection of protein folding and degradation pathways that operate within, and across, cellular compartments (Labbadia and Morimoto, 2015a). Within the PN, the heat shock response (HSR) acts as the main inducible response to protein misfolding in the cytosol/nucleus (Gomez-Pastor et al., 2018). The HSR is coordinated by the transcription factor HSF1, and results in increased protein folding, disaggregation and degradation capacity through elevated levels of molecular chaperones (Gomez-Pastor et al., 2018). Consistent with a central role for proteostasis in promoting healthy ageing, increased HSF1 activity protects against age-associated protein aggregation and extends longevity, while reduced HSF1 activity accelerates proteostasis collapse and tissue degeneration (Alavez et al., 2011; Hsu et al., 2003; Morley and Morimoto, 2004).

Changes in the composition and activity of the PN are thought to increase susceptibility to age-related protein aggregation (Hipp et al., 2019). In particular, it has become apparent that developmental and reproductive signals promote the programmed repression of the HSR during early adulthood, thereby leaving cells vulnerable to proteostasis collapse later in life (Ben-Zvi et al., 2009; Labbadia and Morimoto, 2015b; Shemesh et al., 2013).

In *Caenorhabditis elegans*, mild impairment of the mitochondrial electron transport chain (ETC) during development, a time of heightened mitochondrial biogenesis (Tsang and Lemire, 2002), has been shown to robustly extend lifespan (Dillin et al., 2002; Rea et al., 2007), enhance the activity of the HSR and suppress age-related proteostasis collapse (Labbadia et al., 2017). In addition, impaired mitochondrial function has been shown to increase the expression of HSF1

target genes in yeast, worms, flies, and human cells (Boos et al., 2019; Borch Jensen et al., 2017; Kim et al., 2016; Matilainen et al., 2017). While these observations establish an important connection between mitochondria, HSF1 and cytosolic proteostasis, it remains unclear how developmental changes in ETC function are coupled with HSF1 activity to protect against age-related proteostasis collapse.

Here, we investigate the impact of reduced ETC function on HSF-1 activity, the expression of HSF-1 target genes and age-associated protein aggregation in *C. elegans*. We find that in response to reduced ETC function, two variants of the PP2A serine/threonine protein phosphatase complex generate a de-phosphorylated, mitochondrial stress-specific variant of HSF-1. This safeguards the ageing cytosol against protein aggregation through the selective up-regulation of small heat shock proteins (sHSPs). Furthermore, we show that over-expression of the catalytic subunit of PP2A is sufficient to recapitulate this protective response and suppress age-related protein aggregation without mitochondrial stress. Our findings suggest that mitochondria can actively remodel the cytosolic proteostasis network to meet challenges early in life and that manipulating these pathways may be an effective way to suppress age-related protein conformational disease.

Results

Reduced ETC function enhances the expression of a distinct sub-set of HSF-1 target genes

Mild ETC impairment during *C. elegans* development enhances stress resistance and suppresses cytosolic protein aggregation in an HSF-1 dependent manner (Labbadia et al. 2017). To identify the factors that act downstream of ETC impairment and HSF-1 activation to suppress cytosolic

protein aggregation, we asked which HSF-1 target genes exhibit increased expression in response to mild inhibition of ETC complex IV. We used available RNA-seq and ChIP-seq data (Li et al., 2016) to compile a list of proteostasis network genes that are directly regulated by HSF-1 in *C. elegans*, and profiled their expression under basal conditions and in response to heat shock (33°C, 30 min) at day 3 of adulthood in control (empty vector (EV) RNAi (L4440)) or ETC compromised worms. ETC inhibition was achieved through RNAi against the complex IV subunit, *cox-6c*, using conditions previously shown to protect against age-related protein aggregation without causing developmental delay or sterility (Labbadia et al., 2017).

Unlike general protein folding stress caused by acute heat shock, exposure to *cox-6c(RNAi)* enhanced the induction of a select subset of HSF-1 target genes, both basally and in response to stress (Figure 1A). Knockdown of *cox*-6c induced the small heat shock protein genes *hsp-16.11*, *hsp-16.2* and *hsp-16.48*, the HSP70 homologues *hsp-70* and *hsp-70b*, and the BAG family nucleotide exchange factor and HSP70 co-chaperone, *unc-23*, 2 to 3-fold on day 3 of adulthood compared to EV controls (Figure 1A). These selective effects were not due to the fact that other HSF-1 target genes were not inducible, as nearly all genes tested were elevated ≥ 2-fold by heat shock on day 3 of adulthood (Figure S1A). Furthermore, the response to ETC inhibition was distinct from that induced by a general mild stress caused by transient exposure to elevated maintenance temperatures (Figure S1B). In addition, worms expressing a single copy of mcherry under the control of the HSF-1 dependent *hsp-16.2* promoter, exhibited increased intestinal fluorescence on day 3 of adulthood following *cox-6c(RNAi)* treatment (Figure 1B). Reporter activity was also increased upon genetic or pharmacological perturbation of ETC complexes I, II, III and V, impairment of mitochondrial import or disruption of mitochondrial protein folding (Figure 1B and S1C). However, chronic mitochondrial stress resulting from mutations that that

inhibit ubiquinone synthesis (*clk-1(qm30)*) or germline stem cell proliferation (*glp-1(e2144ts)*) did not increase HSF-1 activity (Figure S1D and S1E). Together, these data demonstrate that acute perturbation of mitochondrial function enhances HSF-1 activity and elevates the expression of a distinct sub-set of HSF-1 target genes.

To determine precisely when mitochondrial stress increases HSF-1 activity in adulthood, we exposed worms to EV control or *cox-6c(RNAi)*, starting at the first larval stage (L1), and quantified gene expression at days 1 – 4 of adulthood. As expected, *hsf-1* mRNA levels were unaltered by progression through adulthood, or exposure to *cox-6c(RNAi)* (Figure 1C) (Labbadia et al., 2017; Labbadia and Morimoto, 2015b). In contrast, by day 2 of adulthood, the levels of all three *hsp-16* genes was elevated by *cox-6c(RNAi)* treatment, while the expression of *hsp-70*, *hsp-70b* and *unc-23* was increased by *cox-6c(RNAi)* on day 3 and day 4 of adulthood (Figure 1C). These data indicate that reduced ETC function in development leads to elevated levels of select HSF-1 target genes in reproductively mature (D2 adulthood onward) adults, with small heat shock protein (sHSP) encoding genes the primary responders to ETC stress.

ETC impairment increases HSF-1 activity through a mechanism that is distinct from previously described stress responses

The induction of *hsp-16* and *hsp-70* genes upon *cox-6c(RNAi)* is strikingly similar to the induction of sHSP genes by DAF-16 and ATFS-1 in response to impaired insulin/IGF-1 signaling (IIS) or activation of the mitochondria-to-cytosolic stress response (McSR) respectively (Hsu et al., 2003; Kim et al., 2016). In addition mitochondrial dysfunction has been shown to activate a xenobiotic stress response (XSR) that is dependent on the transcription factor NHR-45 and that is also associated with elevated levels of sHSPs (Mao et al., 2019). To test whether ETC perturbation may be mimicking these responses, and therefore regulating HSF-1 activity through similar

mechanisms, we exposed *hsp-16.2*p*::mcherry* reporter animals to control conditions or *cox-6c(RNAi)* whilst simultaneously knocking down *daf-16, atfs-1* or *nhr-45*. Knockdown of these transcription factors did not suppress activation of the *hsp-16.*2p::mcherry reporter by *cox-6c(RNAi)* but did reduce the levels of DAF-16 and potently suppress the UPR^{mt} and XSR (Figure 1D and S1F-I). In fact, similar to previous reports (Sorrentino et al., 2017; Wu et al., 2018), both *daf-16(RNAi)* and *atfs-1(RNAi)* increased reporter activity, most likely by enhancing the overall levels of mitochondrial stress. Together, our data show that mild ETC impairment selectively induces a sub-set of HSF-1 target genes in adulthood through a mechanism that is distinct from those previously described.

ETC inhibition suppresses age-related proteostasis collapse in the cytosol through increased levels of small heat shock proteins

Our findings suggest that reduced ETC function protects against age-related protein aggregation in the cytosol through a highly distinct sub-network of HSF-1 regulated chaperones. To determine which of these is required for protection against age-related cytosolic proteostasis collapse, we took advantage of well-described proteostasis sensors expressing polyglutamine or metastable paramysoin in the intestine or body wall muscles, as well as a previously described thermal stress recovery assay (Labbadia et al., 2017; Morley et al., 2002; Prahlad and Morimoto, 2011).

We knocked down *hsp-16, hsp-70,* or *unc-23* in combination with EV control or *cox-6c(RNAi)* and scored susceptibility to polyglutamine aggregation, paralysis (a proxy for proteotoxicity caused by polyglutamine or paramyosin aggregation) and survival following transient heat shock (a proxy for dealing with widespread endogenous protein misfolding) during early adulthood. As expected, polyglutamine aggregation increased with age in both intestine and muscle and was reduced by *cox-6c(RNAi),* as evidenced by a shift from punctate structures to a

more diffuse fluorescent signal in aged animals (Figure S2A and 2A-D). Similarly, *cox-6c(RNAi)* also suppressed age-related paralysis caused by polyglutamine proteins and metastable paramyosin, and increased survival following heat shock (Figure 2E-G, Table S1).

Knockdown of *hsp-70*, *hsp-70b* or *unc-23* did not alter polyglutamine aggregation in intestine or muscle, had no effect on age-related paralysis, and did not modify survival following thermal stress in EV or *cox-6c(RNAi)* treated worms (Figure S2E-K and Table S1). In contrast, RNAi against *hsp-16* genes suppressed the ability of *cox-6c(RNAi)* to protect against polyglutamine aggregation in both intestine and muscle, decreased the effect of *cox-6cc(RNAi)* on proteotoxicity (paralysis), and diminished the impact of *cox-6c(RNAi)* on recovery from heat stress, albeit to a lesser degree than *hsf-1(RNAi)* in all cases (Figure 2A-G, S2A-D and Table S1). Collectively, our data reveal that in response to mild ETC impairment, increased HSF-1 activity primarily protects against protein misfolding, aggregation and toxicity through elevated levels of sHSPs.

LET-92 couples ETC perturbation with increased basal HSF1 activity

To understand how mitochondria influence HSF-1 activity, we hypothesized that factors known to mediate mito-nuclear communication may be important for promoting HSF-1 activity. To test this, we screened a candidate RNAi library (Supplemental table S3) targeting genes previously demonstrated to mediate phenotypic or molecular responses to chemical, microbial or genetic perturbation of mitochondrial function in *C. elegans* (Govindan et al., 2015; Liu et al., 2014; Munkacsy et al., 2016; Shore et al., 2012), for enhancers or suppressors of HSF-1 activity in response to *cox-6c(RNAi)*. We identified 16 genes (including *hsf-1*) that enhanced or suppressed HSF-1 activity ≥ 2-fold on day 3 of adulthood compared to *cox-6c(RNAi)* alone (Figure 3A). We then counter-screened our hits for their effects on the induction of the UPR^{mt} and UPR^{ER}. In

addition to *hsf-1*, only one other gene, *let-92*, which encodes the catalytic subunit of the PP2A serine/threonine protein phosphatase complex, suppressed HSF-1 activity without affecting activation of the UPR^{ER} or UPR^{mt} reporters (Figure 3A-C and S3A). Notably, *let-92* was previously identified as a mediator of lifespan in ETC compromised *isp-1(qm150)* mutants, and as an enhancer of the oxidative stress response (Shore et al., 2012). Although dispensable for UPR^{mt} activation by *cox-6c(RNAi)*, we did find that *let-92(RNAi)* modestly reduced UPR^{mt} activation in response to treatment with the complex III inhibitor, antimycin A (Figure S3B), as previously reported (Shore et al., 2012).

To test whether *let-92* is a general regulator of HSF-1 activity, we assessed the effect of *let-92(RNAi)* on the activation of HSF-1 by heat shock on day 3 of adulthood. *let-92(RNAi)* had no effect on the ability of heat shock to activate HSF-1 (Figure S3C and E). However, as with ETC perturbation, *let-92* was required for full activation of HSF-1 upon inhibition of mitochondrial protein import or perturbation of mitochondrial protein folding (Figure S3D and F). Together, these experiments demonstrate that *let-92* regulates HSF-1 activity specifically in response to mitochondrial stress.

Finally, we tested whether *let-92* is required for *cox-6c(RNAi)* to increase the expression of endogenous HSF-1 target genes. Exposure to *let-92(RNAi)* reduced *let-92* mRNA levels by approximately 50% at day 3 of adulthood without altering the potency of *cox-6c(RNAi)* (Figure S3G). Consistent with our reporter experiments, *let-92* was necessary for *cox-6c(RNAi)* to increase the basal expression of HSF-1 target genes, but not the UPR^{mt} marker, *hsp-6* (Figure 3D). Knockdown of *let-92* had no significant effect on the expression of HSF-1 target genes in EV controls, with the exception of *unc-23*, which was elevated 2-fold (Figure 3D).

Next, we tested the effect of *let-92(RNAi)* on the induction of HSF-1 target genes following heat shock. Surprisingly, *let-92(RNAi)* had no effect on the induction of HSF-1 targets following heat shock in EV control or *cox-6c(RNAi)* worms, with the exception of *hsp-70b*, whose expression was reduced approximately 2-fold in *cox-6c(RNAi)* worms, and *hsp-70,* whose expression was elevated 1.5-fold exclusively in EV control worms (Figure 3E). These findings indicate that different mechanisms regulate the basal and stress induced expression of HSF-1 target genes in response to mitochondrial stress and suggest that *let-92* primarily plays a role in promoting basal HSF-1 activity.

Mitochondria control HSF-1 activity through specific forms of the PP2A complex

As *let-92* encodes for the catalytic subunit of the PP2A complex, we next sought to determine which other PP2A subunits *let-92* cooperates with to regulate HSF-1. Along with LET-92, PP2A forms a holoenzyme with a single scaffold subunit, PPP2R1A/PAA-1, and one of several possible regulatory subunits, which determine substrate specificity (Raman and Pervaiz, 2019).

Therefore, we individually knocked-down all known *C. elegans* PP2A subunits in combination with *cox-6c(RNAi)* and quantified the effect on HSF-1 activity. Knockdown of both *let-92* and the scaffold subunit, *paa-1,* suppressed the activation of HSF-1 by *cox-6c(RNAi)* to a similar extent (Figure 3F). In addition, the B55 family regulatory subunit, *sur-6/PPP2R2A,* and the B72 family regulatory subunit, *rsa-1/PPP2R3C,* also blunted HSF-1 activation by *cox-6c(RNAi)* (Figure 3F). RNAi against other B subunits (*pptr-1, pptr-2, F43B10.1* and *T22D1.5*) did not alter HSF-1 activity in response to *cox-6c(RNAi),* despite the fact that mRNA of these targets was knocked down with the same efficiency as for *let-92* (Figure S3G and H). We did not find evidence that ETC impairment appreciably alters the expression of *paa-1, let-92, sur-6,* or *rsa-1* (Figure S3I) or that mitochondria-mediated HSF-1 activation is dependent on known PP2A

regulators that have previously been linked to mitochondrial stress (Ahn et al., 2007; Raman and Pervaiz, 2019; Schiavi et al., 2015; Yang et al., 2018) (Figure 3G and S3N). Furthermore, activation of the UPR^{mt} or UPR^{ER} was unaffected by knockdown of PP2A subunits, with the exception of *rsa-1(RNAi)*, which reduced induction of the UPR^{ER} (Figure S3J-M).

Our data suggest that mitochondrial stress acts through two distinct forms of the PP2A complex (B55-PP2A and B72-PP2A) to regulate HSF-1 activity and protect against cytosolic protein aggregation. Our data place PP2A and HSF-1 downstream of mitochondrial stress as part of the mechanisms through which cells safeguard the cytosolic proteome.

let-92 is necessary for mild ETC dysfunction to suppress age-related proteostasis collapse

Given that *let-92* is required for mitochondrial stress to enhance HSF-1 activity, we next asked whether *let-92* is required for ETC impairment to suppress age-related cytosolic proteostasis collapse.

We found that *let-92(RNAi)* did not alter transgene levels (Figure S4A and B), but did accelerate polyglutamine aggregation and toxicity in the intestine and body wall muscles compared to EV controls (Figure 4A-D). Furthermore, *let-92(RNAi)* shortened lifespan compared to EV controls (Figure 4F), consistent with previous findings (Shore et al., 2012). However, *let-92(RNAi)* had no effect on the ability of animals to recover from thermal stress on day 3 of adulthood, consistent with our observations that *let-92* is not required for the HSR (Figure 4E).

In addition to its effects on proteostasis in wild-type animals, *let-92(RNAi)* reduced the ability of *cox-6c(RNAi)* to suppress polyglutamine aggregation and toxicity in the intestine and body wall muscles and extend lifespan, but did not alter the survival of *cox-6c(RNAi)* treated animals following thermal stress (Figure 4A-F). Together, these data indicate that *let-92* is

necessary for both the general maintenance of proteostasis, and for ETC impairment to suppress cytosolic proteostasis collapse.

PP2A generates a mitochondrial stress activated form of HSF-1

To understand precisely how PP2A regulates HSF-1 activity, we first asked whether *let-92(RNAi)* alters *hsf-1* mRNA levels and found that this was not the case (Figure S5A). We next asked whether LET-92 directly associates with HSF-1, using worms expressing a single-copy of a functional HSF-1-GFP fusion protein (HSF-1::GFP) (Li et al., 2016). We found that LET-92 co-immunoprecipitated with HSF-1::GFP under *cox-6c(RNAi)* conditions, but not EV control or *let-92;cox-6c(RNAi)* conditions (Figure 5A), suggesting that LET-92 directly associates with HSF-1 in response to mitochondrial stress.

Given that HSF-1 is constitutively phosphorylated (Ooi and Prahlad, 2017), we next hypothesized that, contrary to classical models of HSF-1 activation, dephosphorylation by PP2A may increase HSF-1 activity. Consistent with our previous observations (Labbadia et al., 2017), we observed that the levels and mobility of HSF-1::GFP does not shift upon SDS-PAGE in response to *cox-6c(RNAi)* (Figure 5A). Given that GFP is a large tag, we hypothesized that a more subtle change in phosphorylation may be masked by standard SDS-PAGE. To test this, we used a Phos-tag SDS-PAGE system to exacerbate migration events caused by the presence of phosphorylated residues (Kinoshita et al., 2009).

Compared to EV controls, HSF-1 migrated significantly faster in *cox-6c(RNAi)* worms on the Phos-tag gel (Figure 5B), and this was suppressed by *let-92(RNAi)* (Figure 5B), suggesting that HSF-1 is dephosphorylated in response to ETC perturbation in a *let-92* dependent manner.

To understand how dephosphorylation influences HSF-1 function, we used chromatin-IP (ChIP) followed by real-time quantitative PCR (RTQPCR) to quantify relative enrichment of HSF-1 and RNA Pol-2 at specific promoters (Figure S5B) following treatment with EV or *cox-6c(RNAi)* in combination with *let-92(RNAi)*.

Consistent with our gene expression analyses, exposure of worms to *cox-6c(RNAi)* increased levels of RNA Pol-2 at the promoters of *hsp-16.11, hsp-16.2, hsp-16.48, hsp-70, hsp-70b* and *unc-23*, but not at the promoters of *hsp-1, hsp-90, hsp-110,* or the non-HSF-1 target gene, *cdc-42* (Figure 5C). Furthermore, the levels of RNA Pol-2 recovered were substantially higher than those recovered using IgG alone. Similarly, *cox-6c(RNAi)* resulted in the same pattern of HSF-1::GFP promoter enrichment, and HSF-1::GFP was not detected at levels above IgG control or at the *cdc-42* promoter (Figure 5C). Knockdown of *let-92* had no effect on HSF-1 or RNA Pol-2 association with target promoters compared to EV controls, with the exception of the *unc-23* promoter, which exhibited increased RNA Pol-2 and HSF-1 binding in *let-92(RNAi)* worms (consistent with our gene expression data (Figure 3D)). However, *let-92(RNAi)* did strongly abrogate HSF-1 and RNA Pol-2 levels specifically at the promoters of HSF-1 target genes induced by *cox-6c(RNAi)* (Figure 5C). Together, these experiments reveal that PP2A generates a mitochondrial stress-activated, hypo-phosphorylated, variant of HSF-1 that is markedly different from that generated by heat shock, and that preferentially binds to the promoters of distinct HSF-1 target genes (Labbadia et al., 2017).

To provide insight into the functional impact of HSF-1 hypo-phosphorylation, we took advantage of worms expressing GFP under the control of an HSF-1 target promoter (*Y94H6A.10*p) that has been modified to remove regulatory sequences, with the exception of two heat shock elements (HSEs), the canonical binding motifs for HSF-1 (Li et al., 2016). While the levels of a

constitutively expressed co-expression marker (unc-119::mcherry) were unaltered across conditions (Figure S5D), we observed that heat stress, but not mitochondrial stress, induced the HSE::GFP reporter in an HSF-1 dependent manner. This suggests that hypo-phosphorylated HSF-1 does not bind indiscriminately to HSEs and is functionally distinct from hyper-phosphorylated (heat activated) HSF-1 (Figure 5D and S5D).

To complement our reporter experiments we also used ChIP-QPCR to assess HSF-1 levels at the promoters of two genes known to be bound by HSF-1 (Li et al., 2016); one up-regulated exclusively by heat shock (*Y94H6A.10*) and one up-regulated exclusively by mitochondrial stress (*Y55F3AR.2*) (Figure S5C). Hyper-phosphorylated (heat activated) HSF-1 bound exclusively to the *Y94H6A.10* promoter while hypo-phosphorylated (mitochondrial stress activated) HSF-1 bound exclusively to the *Y55F3AR.2* promoter (Figure 5E). Together with our reporter experiments, these data suggest that mitochondrial stress activated HSF-1 and heat activated HSF-1 are functionally distinct.

Over-expression of *let-92* is sufficient to selectively induce the expression of HSF-1 target genes and protect against age-related proteostasis collapse

Finally, we wondered whether we could uncouple ETC impairment from the suppression of age-related protein aggregation by increasing PP2A activity. To this end, we over-expressed *let-92* using the ubiquitously expressed *sur-5* promoter and examined the effects on age-related protein aggregation. Compared to wild type controls, three independent *let-92* over-expression lines (*let-92 OE)* robustly suppressed age-related polyglutamine aggregation without altering transgene levels (Figure 6A, 6B and S6A). In contrast, none of the *let-92 OE* lines tested enhanced survival following transient exposure to thermal stress, consistent with a primary role for *let-92* in regulating basal HSF-1 activity (Figure S6B and Table S1).

We next checked the expression of HSF-1 target genes in *let-92 OE* worms. Strikingly, as observed upon *cox-6c(RNAi), let-92 OE* had little effect on the majority of HSF-1 target genes tested (Figure 6C). However, *let-92 OE* did increase the expression of *hsp-16.11, hsp-16.2, hsp-16.48, hsp-70, hsp-70b* and *unc-23*, 2 to 3-fold, levels comparable with those seen in response to *cox-6c(RNAi)* (Figure 6C). This suggests that increased levels of LET-92 are sufficient to mimic the effect of *cox-6c(RNAi)* treatment on HSF-1 activity and age-related proteostasis collapse.

Next, we tested whether the ability of *let-92 OE* to suppress polyglutamine aggregation is dependent on *hsf-1* and *hsp-16s*. As expected, wild type controls exhibited an age-dependent increase in polyglutamine aggregation that was profoundly suppressed by *let-92 OE* (Figure 6D). In contrast, *hsf-1(RNAi)* accelerated polyglutamine aggregation and suppressed the ability of *let-92 OE* to maintain proteostasis (Figure 6D). Similarly, *hsp-16.11* and *hsp-16.48(RNAi)*, but not *hsp-16.2(RNAi),* were also partially required for *let-92 OE* to suppress polyglutamine aggregation (Figure 6E and S6D-F).

Finally, we tested whether *let-92 OE* can extend longevity. We found that *let-92 OE* only modestly extended lifespan compared to wild type animals (Figure 6F) and increased egg-retention and bagging (Figure S6C). This suggests that while *let-92 OE* is sufficient to recapitulate the ETC-HSF-1 stress response, maintain proteostasis and extend lifespan, the effects of PP2A on ageing in the absence of ETC impairment are less pronounced.

Together, our data suggest that in response to ETC impairment, two variants of the PP2A complex (B55/B72) bind to and dephosphorylate HSF-1. This generates a mitochondrial stress-activated variant of HSF-1, which preferentially drives the expression of sHSPs, thereby safeguarding the ageing cytosolic proteome (Figure 7).

Discussion

Mitochondria have emerged as important regulators of HSF1 activity and cytosolic proteostasis (Boos et al., 2019; Kim et al., 2016; Labbadia et al., 2017). However, the mechanisms by which mitochondria can control susceptibility to cytosolic protein aggregation in adulthood are unknown. Furthermore, the relationship between mitochondrial function and ageing is highly complex, with the pathways that promote healthy ageing downstream of mitochondrial perturbation, poorly understood. (Sun et al., 2016). Here, we provide evidence that in *C. elegans*, reduced ETC function during development protects against age-related proteostasis collapse and promotes longevity through a mitochondrial stress-specific variant of HSF-1.

Our data suggests that mitochondria primarily protect the cytosol against age-related proteostasis collapse through elevated levels of sHSPs. Increased levels of sHSPs have also been linked to enhanced proteostasis and increased longevity following reduced IIS (Hsu et al., 2003). However, the levels of various sHSPs also increases with age in wild type *C. elegans*, thereby protecting against age-related proteotoxicity by sequestering toxic protein oligomers into large protein aggregates (Walther et al., 2015). Consistent with this, we also observe that *hsp-16.2* expression increases during early adulthood. It is unclear why *hsp-16.2*, but not other HSF-1 targets, is elevated in early adulthood. However, the expression of sHSPs has been shown to be regulated by promoter accessibility and DAF-16 activity (Hsu et al., 2003; Labbadia and Morimoto, 2015b). Therefore, it is possible that increased *hsp-16.2* expression with age, reflects changes in chromatin architecture and/or cofactor function not observed at other heat shock genes. Collectively, our observations suggest that sHSPs can protect against age-related protein aggregation through diverse strategies that are possibly dependent on the stage of life, status of the proteome and composition of the PN.

Intriguingly, not all sHSPs are equally effective in suppressing protein aggregation (Vos et al., 2016; Vos et al., 2010). In both *Drosophila* S2 cells, and HEK293 cells, the ability to potently suppress polyglutamine aggregation or HSP70 mediated refolding of heat denatured luciferase, was restricted to distinct, non-overlapping, sHSP family members (Vos et al., 2016; Vos et al., 2010). Similarly, our findings demonstrate that in response to ETC impairment, specific *C. elegans* sHSPs are mobilized to protect against protein aggregation and enhance stress resistance. Together, these observations suggest that cells have evolved a functionally diverse range of sHSPs that can be deployed, as and when required, to recognize and nullify disparate misfolded protein species, thereby efficiently maintaining proteostasis in response to assorted forms of environmental and physiological stress.

Given that sHSPs are non-ATP dependent chaperones that sequester misfolded proteins until they can be refolded by the ATP-dependent HSP70 machinery (Haslbeck et al., 2019), we propose that cells employ a distinct HSF-1 variant to shift the composition of the PN to favor non-ATP dependent "holdases" as the primary line of defence against the threat of misfolded proteins, possibly to counter the fact that protein degradation pathways are impaired and that ATP levels are reduced (Livnat-Levanon et al., 2014; Segref et al., 2014). The fact that we also see an induction of HSP70 family members suggests that cells prepare for immediate refolding and/or clearance of sHSP-sequestered cytosolic proteins once ATP-levels are restored.

In contrast to the heat shock response, we find that increased HSF-1 activity following ETC disruption is associated with the de-phosphorylation of HSF-1. While increased HSF1 activity is classically associated with hyper-phosphorylation, the impact of phosphorylation on HSF1 activity is poorly understood. However, it is clear that HSF1 activity and phosphorylation can be uncoupled, with a phospho-deficient mutant of HSF1 shown to more potently induce the

expression of chaperone genes in response to heat shock in mammalian cells (Budzynski et al., 2015). Furthermore, it has been shown that in human non-small cell lung carcinoma, increased HSF1 activity is associated with a hypo-phosphorylated form of HSF1 that promotes cancer cell survival (Asano et al., 2016). These observations, coupled with our findings, suggest that de-phosphorylation of HSF-1 may be a general mechanism for stably increasing HSF1 activity in response to metabolic stress.

While we have shown that HSF-1 binds more readily to the promoters of a specific sub-set of targets following ETC impairment, it remains unclear what drives this specificity. A recent study demonstrated that the chromatin remodeler, ISW-1, is important for ETC stress to elevate levels of *hsp-16s* during development (L4 stage animals) (Matilainen et al., 2017), suggesting that a permissive chromatin state, set before the onset of mitochondrial stress, may prime specific promoters for HSF-1 binding. However, our data demonstrate that dephosphorylated HSF-1 does not bind indiscriminately to available HSEs and does not bind to the same target promoters as hyper-phosphorylated (heat activated) HSF-1 (although some promoters are bound by both HSF-1 variants). This raises the possibility that PP2A-mediated dephosphorylation functionally distinguishes mitochondrial stress activated HSF-1 from heat activated HSF-1 in order to promote preferential binding at *hsp-16* and *hsp-70* genes. Alternatively, it remains possible that PP2A might alter the activity of mitochondrial stress-specific co-factors that cooperate with HSF-1 to promote binding at specific promoters. Future work to identify the exact factors and mechanisms that determine the differential promoter preferences of HSF-1 following heat shock or mitochondrial stress, will be important to completely understand exactly how mitochondria remodel the PN so precisely using a variant of HSF-1.

In addition to our findings in worms, it has also been reported that PP2A associates with, and dephosphorylates, HSF-1 in cancer cells, and that dephosphorylation of the metabolic sensor AMPK by PP2A is regulated by HSF1 in mice (Su et al., 2019). These observations suggest a highly complex interplay between PP2A activity, metabolic status and proteostasis, and raise the prospect that activation of the PP2A-HSF1 axis may drive a general adaptive response to metabolic remodeling.

Finally, we have shown that increased HSF-1 activity and maintenance of cytosolic proteostasis are associated with increased lifespan in response to reduced ETC function. However, we find that HSF-1 activity is also increased by inhibition of complex II or mitochondrial import, neither of which extend lifespan. Furthermore, while *let-92 OE* potently suppressed proteostasis collapse in an HSF-1 dependent manner, it did not extend lifespan to the same extent as *cox-6c(RNAi)*. This is similar to observations regarding the relationship between the UPR^{mt} and ageing (Bennett et al., 2014), and suggests that future work to understand exactly why increased HSF-1 activity is not sufficient to extend lifespan under certain conditions and is less potent than when observed in combination with ETC perturbation, will be crucial for us to properly understand the interplay between metabolism, HSF-1, proteostasis and ageing. Nevertheless, our work complements an emerging appreciation that mitochondria are central regulators of cytosolic protein quality control pathways (Boos et al., 2019; Kim et al., 2016; Wang and Chen, 2015; Wrobel et al., 2015) and demonstrates that mitochondrial regulation of cytosolic proteostasis can positively influence long-term health.

In conclusion, our work has revealed the mechanism by which mitochondria signal to HSF-1 and maintain cytosolic proteostasis. Future work to identify small molecule activators of PP2A, and

investigate their long-term effects in models of ageing, may lead to new treatments for age-related protein conformational disorders.

Acknowledgements

We are grateful to members of the IHA, particularly the Gems lab, for sharing equipment and ideas, and for helpful comments and discussions. We also thank the Poole and Barrios labs for access to RNAi libraries, and the Biosciences Molecular Biology Facility for access to core equipment. This work was supported by a BBSRC David Phillips Fellowship [BB/P005535/1], An Academy of Medical Sciences/Wellcome Trust/Government Department of Business, Energy and Industrial Strategy/British Heart Foundation/Diabetes UK Springboard Award [SBF004\1051] and a Wellcome Trust Strategic [ISSF3/H17RCO/NG18] Award to John Labbadia.

Author contributions

Conceptualization, J.L.; Methodology, J.L.; Validation, J.L., R.W. and M.L.; Formal Analysis, J.L., R.W., and M.L.; Investigation, J.L., R.W., M.L., R.I.W. and A.M.; Resources, J.L.; Writing-Original Draft, J.L.; Writing-Review & Editing, J.L., R.W., M.L., R.I.W. and A.M.; Visualization, J.L.; Supervision, J.L., R.W. and M.L.; Project Administration, J.L.; Funding Acquisition, J.L.

Declaration of Interests

The authors declare no competing interests

Figure titles and legends

Figure 1: ETC perturbation enhances the expression of a sub-set of HSF-1 target genes through a pathway that is distinct from previously described stress responses

A – Relative mRNA levels of HSF-1 target genes at day3 of adulthood following exposure to empty vector (EV) control (L4440) or *cox-6c(RNAi)* for 4 biological replicates (1-4) per treatment group.

B – Representative images and quantification of mCherry fluorescence of day 3 adult worms expressing a single-copy of an *hsp-16.2*p::mcherry transgene (TJ3002). TJ3002 worms were exposed to EV control conditions or RNAi against indicated mitochondrial genes. Values plotted are the mean fluorescence intensity of at least 15 worms per treatment group.

C – Relative mRNA levels at different days of adulthood in EV control or *cox-6c(RNAi)* worms. Values plotted are the mean of 4 biological replicates.

D – Representative images and quantification of mCherry fluorescence of D3 adult TJ3002 worms exposed to EV control RNAi or *cox-6c(RNAi)* in combination with *hsf-1(RNAi), daf-16(RNAi), atfs-1(RNAi)* or *nhr-45(RNAi)*. Values plotted are the mean fluorescence intensity of at least 15 worms per treatment group.

Scale bars = 250 μM and statistical significance was calculated by: (**A**) two-tailed, unpaired Student's *t*-test, with FDR-corrected *P*-values reported; (**B**) One-way ANOVA with Dunnett's post-test comparison of groups to EV control; (**C and D**) two-way ANOVA with post analysis pair-wise comparison of groups. All error bars represent SEM. * $p < 0.05$, ** $p < 0.01$, *** $p < 0.001$.

Figure 2: Reduced ETC activity safeguards cytosolic proteostasis in different tissues through elevated levels of small heat shock proteins

A – Mean day of adulthood at which 50% of the population exhibit intestinal polyglutamine (Q44)::YFP aggregates (Agg50) in worms grown on EV control or *cox-6c(RNAi)* combined with RNAi against *hsf-1* or HSF-1 target genes. Values plotted are the mean of 4 biological replicates.

B - Representative images of worms expressing intestinal polyQ44::YFP at day 6 of adulthood following exposure to EV control or *cox-6c(RNAi)* combined with RNAi against *hsp-16* genes. Scale bar = (B) 250 µM.

C - Quantification of body wall muscle Q35::YFP aggregation with age in worms grown on EV control (solid lines/bars) or *cox-6c(RNAi)* (broken lines/open bars) combined with RNAi against *hsp-16* genes or *hsf-1*.

D – Representative images of worms expressing body wall muscle Q35::YFP on day 3 of adulthood, following exposure to EV control or *cox-6c(RNAi)* combined with RNAi against *hsp-16* genes. Panels contain zoomed in images of the head area. Scale bar = 100 µM.

E and F – Paralysis of worms expressing (**E**) polyQ35::YFP or (**F**) metastable paramysoin (*unc-15ts)* in body wall muscle cells at different days of adulthood following growth on EV control (solid lines) or *cox-6c(RNAi)* (broken lines) combined with RNAi against *hsp-16* genes or *hsf-1*. Values plotted are the mean of 4 biological replicates.

G – Survival (n > 100 per group) at 20°C of worms following 4 hour heat shock at 35°C on day 3 of adulthood after growth on EV control (solid lines) or *cox-6c(RNAi)* (broken lines) combined with RNAi against *hsp-16* genes or *hsf-1*.

Statistical significance was calculated by: (**A**) two-way ANOVA with post-analysis pairwise comparison of groups and (**G**) Mantel-Cox Log-rank test. All error bars represent SEM. * $p < 0.05$, ** $p < 0.01$, *** $p < 0.001$.

Figure 3: *let-92* is required for increased basal HSF-1 activity following ETC impairment

A – Relative fluorescence intensity of transcriptional reporters of the HSR (*hsp-16.2p::mcherry*), UPR^{mt} (*hsp-6p::gfp*) and UPR^{ER} (*hsp-4p::gfp*) on day 3 of adulthood. Fold changes were calculated relative to *cox-6c(RNAi)* (HSR, UPR^{mt}) or *hsp-3(RNAi)* (UPR^{ER}) treatments and derived from > 20 worms per treatment group.

B-C Representative images of day 3 adult *hsp-16.2p::mcherry*, *hsp-6p::gfp*, and *hsp-4p::gfp* reporter lines following growth on EV control, *cox-6c(RNAi)*, or *hsp-3(RNAi)* combined with *let-92(RNAi)*.

D & E – Expression of HSF-1 target genes under (**D**) basal conditions or (**E**) following heat shock (33°C, 30 min) on day 3 of adulthood, after growth on EV control or *cox-6c(RNAi)* combined with *let-92(RNAi)*. Values plotted are the mean of 4 biological replicates.

F – Representative images and quantification of mCherry fluorescence of day 3 adult *hsp-16.*2p::mcherry worms following growth on EV control, *cox-6c(RNAi)* or *cox-6c(RNAi)* combined with RNAi against specific subunits of the PP2A complex. Values plotted are the mean fluorescence intensity of at least 15 worms per treatment group.

G – Quantification of fluorescence intensity in day 3 adult *hsp-16.2*p::mcherry worms following exposure to EV control RNAi or *cox-6c(RNAi)* in combination with RNAi against PP2A

regulators. Values plotted are the mean fluorescence intensity from at least 15 worms per treatment group.

All scale bars = 250 µM. Statistical significance was calculated by (**D**-**G**) one-way ANOVA with Tukey post-analysis pairwise comparison of groups. All error bars represent SEM. * = $p < 0.05$, ** = $p < 0.01$, *** = $p < 0.001$.

Figure 4: *let-92* is necessary for ETC impairment to protect against age-related proteostasis collapse in different tissues

A and C – Quantification of (**A**) intestinal polyglutamine (Q44)::YFP aggregation, or (**C**) body wall muscle Q35::YFP aggregation, at different days of adulthood in worms grown on EV control or *cox-6c(RNAi)* combined with *let-92(RNAi)*. Values plotted are the mean of (**A**) 4 biological replicates or (**C**) 20 biological replicates. All error bars represent SEM.

B – Representative images of day 4 adult worms expressing intestinal polyQ44::YFP following exposure to EV control or *cox-6c(RNAi)* combined with *let-92(RNAi)*. Scale bar = 250 µM

D – Incidence of paralysis at different days of adulthood in worms expressing polyQ35::YFP in body wall muscle cells and grown on EV control or *cox-6c(RNAi)* combined with *let-92(RNAi)*. Values plotted are the mean of 4 biological replicates and error bars represent SEM.

E and F – Survival (n > 100 per group) following (**E**) 4 hour heat shock at 35°C on day 3 of adulthood, or (**F**) with constant growth at 20°C. Worms were grown on EV control or *cox-6c(RNAi)* combined with *let-92(RNAi)*. Statistical significance was calculated by Mantel-Cox Log rank test. Median lifespans in (**F**) are: EV (L4440) = 18 days (n = 141), *cox-6c(RNAi)* = 23 days

(n = 136), *let-92(RNAi);EV* = 16 days (n = 128), *let-92(RNAi);cox-6c(RNAi)* = 18 days (n = 130). Further information on survival trials is presented in Table S1.

Figure 5: PP2A generates a hypo-phosphorylated form of HSF-1 that exhibits increased binding at a sub-set of HSF-1 target promoters

A – Representative western blots of HSF-1::GFP, LET-92 or alpha-tubulin in inputs or following immunoprecipitation (IP) of HSF-1::GFP from day 3 adult worms grown on empty vector (EV) control, *cox-6c(RNAi), let-92;EV(RNAi)* or *let-92(RNAi);cox-6c(RNAi),* or IP using normal rabbit IgG. N2 wild type animals that do not express HSF-1::GFP were used as a background control.

B – Representative western blots of HSF-1::GFP or alpha-tubulin following Phos-tag SDS-PAGE separation of protein lysates from day 3 adult worms grown on empty vector (EV) control, *cox-6c(RNAi), let-92;EV(RNAi)* or *let-92(RNAi);cox-6c(RNAi)* treated worms.

C – Relative recovery of promoters following ChIP of (top) RNA Pol-2 (AMA-1) or (bottom) HSF-1::GFP at day 3 of adulthood following growth on EV control, *cox-6c(RNAi), let-92(RNAi);EV,* or *let-92;cox-6c(RNAi).* Values plotted are the mean of 4 biological replicates and error bars represent SEM. Statistical significance was calculated by one-way ANOVA with Tukey post analysis pairwise comparison of groups. * = $p < 0.05$, ** = $p < 0.01$. Black lines = % recovery of input obtained with IgG.

D - Representative images and fluorescence quantification of day 3 adult worms expressing GFP under the control of a promoter containing only two heat shock elements (HSEp::GFP) and grown on empty vector (EV) control (L4440), *hsf-1(RNAi)* or *cox-6c(RNAi).* Animals were exposed to

control conditions or heat shock (35°C, 1 hour). Values plotted are the mean fluorescence intensity of at least 15 worms per group. Scale bars = 250 μM.

E - Relative recovery of the *Y94H6A.10* (heat inducible only), *Y55F3AR.2* (mito stress inducible only) or *cdc-42* (non-HSF-1 target) promoters following ChIP of HSF-1::GFP at day 3 of adulthood following exposure to EV control, *cox-6c(RNAi)* or heat shock (35°C, 1 hour). N2 wild type animals that do not express HSF-1::GFP were used as a background control. Values plotted are the mean of 3 biological replicates. Error bars represent SEM. Statistical significance was calculated by one-way ANOVA. * = $p < 0.05$, ** = $p < 0.01$, *** = $p < 0.001$.

Figure 6: Overexpression of *let-92* suppresses age-related proteostasis collapse in an HSF-1 dependent manner

A – Quantification of intestinal polyglutamine(Q44)::YFP aggregation with age in wild type or *let-92* over-expression *(let-92 OE)* worms. Wild type animals were expressing the co-injection marker alone.

B – Representative images of intestinal polyQ44::YFP aggregation at day 4 of adulthood in wild type or *let-92 OE* worms. Scale bar = 250 μM

C – Relative expression of HSF-1 target genes at day 3 of adulthood in wild type (blue bars) or *let-92 OE* (red bars) worms. Values plotted are the mean of 4 biological replicates and error bars represent SEM. Expression levels were normalized to the geometric mean of the housekeeping genes *rpb-2, cdc-42,* and *pmp-3*. Statistical significance was calculated by unpaired, two-tailed Student's t-test. * = $p < 0.05$, ** = $p < 0.01$, *** = $p < 0.001$.

D - Quantification of intestinal polyQ44::YFP aggregation with age in wild type or *let-92 OE* worms exposed to empty vector (EV) control (L4440) or *hsf-1(RNAi)*. Values plotted are the mean of 4 biological replicates and error bars represent SEM.

E – Mean day of adulthood at which 50% of the population exhibit intestinal polyglutamine (Q44)::YFP aggregates (Agg50) in worms grown on EV control or *cox-6c(RNAi)* combined with RNAi against *hsp-16.11, hsp-16.2* or *hsp-16.48*. Values plotted are the mean of 4 biological replicates.

Quantification of intestinal polyglutamine(Q44)::YFP aggregation in wild type or *let-92* over-expression *(let-92 OE)* worms exposed to empty vector (EV) control (L4440) or *hsp-16(RNAi)*. The mean number of days for 50% of the population to exhibit protein aggregates was calculated from 4 biological replicates and plotted.

F – Lifespan (20°C) of wild type and *let-92 OE* worms. Statistical significance was calculated by Log-rank Mantel-Cox test. Median lifespans are: wild type = 16 days (n = 168), *let-92 OE (line 1)* = 17.5 days (n = 106), *let-92 OE (line 2)* = 17.5 days (n = 111), *let-92 OE (line 3)* = 18 days (n = 124). Further survival statistics can be found in Table S1.

Figure 7: A proposed model for the suppression of age-related cytosolic protein aggregation by mitochondria

In response to general protein misfolding, HSF-1 is hyper-phosphorylated and drives the expression of molecular chaperones to promote protein folding activity. In response to mitochondrial dysfunction, cells promote “holdase” activity through a hypo-phosphorylated variant of HSF-1.

STAR Methods

Resource Availability

Lead contact

Further information and requests for resources and reagents should be directed to and will be fulfilled by the Lead Contact, John Labbadia (j.labbadia@ucl.ac.uk).

Materials Availability

Worm strains generated in this study have been deposited to the *Caenorhabditis elegans* genetics center, University of Minnesota, USA.

Data and code availability

Original/source data for all figures in the paper is available upon request from the lead contact. This study did not generate any code, RNA-seq or ChIP-seq datasets. Previously published RNA-seq and ChIP-seq data sets (Li et al., 2016) analyzed within this study are available at Gene Expression Omnibus (GSE81523).

Experimental model and subject details

Unless stated, *C. elegans* strains were maintained at 20°C on NGM plates seeded with OP50 *Eschericia coli* bacteria using previously described methods (Brenner, 1974). Worms over-expressing *let-92* were generated by inserting the *let-92* coding sequence, in frame, downstream of the *sur-5* promoter and upstream of the *unc-54* 3'UTR in the pTG96 vector using Age I and EcoRI restriction sites (SUNY Biotech). This essentially replaced the *sur-5::gfp::NLS* with *let-92.* Transgenic worms were generated by injecting the construct along with a *myo-3p::mcherry* co-injection marker into the germ line of day 1 adult hermaphrodites. The transgene was integrated into the genome using UV integration and worms were outcrossed 11 times before use. A full list

of strains used in this study can be found in the key resources table. RNAi was performed by feeding. Luria Bertani media containing 100 ug/ml ampicillin was inoculated with RNAi bacteria and grown overnight at 37°C (16h). Cultures were then induced with 5 mM IPTG and allowed to grow for a further 3h at 37°C. Following this, cultures were seeded onto 60 mm NGM plates containing 100 ug/ml ampicillin and 1 mM IPTG, and allowed to dry at room temperature for 2 – 3 days. For all combinatorial RNAi experiments, bacterial cultures were OD matched before mixing and plating. RNAi plates were always seeded with bacteria within 1 week of pouring and used for experiments within 1 week of seeding. All RNAi clones were obtained from either the Ahringer or Vidal libraries and sequence verified before use.

Method details

Genetic screen

Candidate RNAi clones were sequenced verified and grown as described above. Following induction, RNAi bacteria were mixed with *cox-6c(RNAi)* at a 1:1 ratio (v/v) to maximise knockdown of target genes and suppress detrimental effects caused by *cox-6c(RNAi)*. For all experiments, bacterial cultures were OD matched before mixing and plating. Approximately 40, bleach synchronized TJ3002 L1 larvae were added to 60 mm RNAi plates seeded with different RNAi/*cox-6c* mixes and allowed to reach day 3 of adulthood. Progeny were removed by transferring worms to new plates on day 2 and day 3 of adulthood. Fluorescence intensity was then quantified in the intestine of individual worms using FIJI. This was repeated using SJ100 and SJ4005 reporter strains for any RNAi clones that altered TJ3002 fluorescence > 2-fold compared to EV;*cox-6c(RNAi)* treated worms. In the case of SJ4005, RNAI clones of interest were mixed with *hsp-3(RNAi)* instead of *cox-6c(RNAi)*. A full list of clones and effects on reporter fluorescence can be found in supplemental table 3.

Heat shock and drug treatments

Worms were heat shocked on 60 mm NGM or RNAi plates by immersing parafilm wrapped plates in a pre-heated water bath at the indicated temperatures. Plates were heat shocked for indicated times and worms were then harvested immediately and snap frozen in liquid nitrogen. For paraquat, antimycin and rotenone treatment, chemicals were dissolved in water (paraquat) or DMSO (antimycin, rotenone) and added to media to a final concentration of 1 mM paraquat, 250 µM Antimycin or 250 µM rotenone before pouring plates. All paraquat, antimycin and rotenone plates were used within 1 week of pouring.

RNA extraction, cDNA synthesis and gene expression analyses

RNA was extracted from approximately 200 adult worms using 250 µL Trizol extraction reagent. Worms were vortexed continuously for 10 minutes and then allowed to rest on ice for another 10 minutes. This was performed 3 times. Following this, 50 µL chloroform was added to Trizol, shaken for 15s by hand, and allowed to stand at room temperature for 3 minutes. Samples were then centrifuged at 13,000 x *g* for 15 minutes. The aqueous phase was then collected, mixed with an equal volume of 70% ethanol, and then added to the center of a RNeasy RNA extraction column. RNA was purified as per manufacturer's instructions using on column DNase I digestion to remove genomic DNA. cDNA was synthesized from 1 µg total RNA using BioRad iScript cDNA synthesis kit as per manufacturer's instructions. Finally, relative mRNA levels were determined by real-time quantitative PCR using BioRad Ssod advanced SYBR green master mix and a BioRad CFX96 thermocycler. Relative mRNA levels were then calculated by standard curve method and gene expression was normalized to the geometric mean of the housekeeping genes *cdc-42, pmp-3,* and *rpb-2.* All primers used can be found in supplemental table 2.

Chromatin immunoprecipitation

Approximately 20,000 – 30,000 bleach synchronized L1 larvae were grown on 10 cm RNAi plates seeded with RNAi bacteria (approx. 500 worms per plate). Progeny were removed at day 2 and day 3 of adulthood by by gravity sedimentation in M9. Eggs and L1 larvae suspended in the "supernatant" were removed and the process was repeated 3 times to ensure the removal of all progeny (confirmed by examining 20 µl aliquots of packed adult worms on a glass slide under a light microscope). Chromatin cross-linking was performed by gently agitating worms in 1% formaldehyde in PBS on a nutator at room temperature for 30 min with intermittent douncing of worms to promote disruption of the cuticle. Cross-linking was quenched by incubation with 125 mM glycine for 10 minutes at room temperature. Worms were then pelleted and washed 3 times with ice-cold FA buffer (50 mM HEPES/KOH pH7.5, 1 mM EDTA, 1% Triton X-100, 0.1% sodium deoxyholate, 150 mM NaCl with Roche Complete protease inhibitors). Worm pellets were then re-suspended in 500 µl of FA buffer and dounce homogenized on ice for 30 – 60 minutes to completely break-up worms. Animals were further broken up by 10 rounds of sonication on high power (30s on, 60s off) using a Bioruptor sonicator (Diagenode). Complete destruction of worms was confirmed by examination of 2 µl of worm chromatin samples under a light microscope and chromatin preps were then centrifuged at 17,000 x *g* for 15 min at 4°C. Chromatin was sheared to 300-500 base pair fragments with an additional 10 rounds of sonication on high power (30s on, 60s off) and shearing efficiency was examined by electrophoresis of 5 µl of reverse cross-linked chromatin on a 1% agarose gel. Pulldowns were set up using 2 mg of protein, 20 µl of protein-G Dynabeads (Invitrogen), and either 5 µl of anti-full length GFP antibody (Clontech, living colors), or 2 µg of anti-AMA-1 antibody (Novus Biological) in FA buffer (1 ml total volume). Pulldowns were then incubated at 4°C overnight on a rotating wheel. Following incubation, protein-G

Dynabeads were washed at room temperature 2 times for 5 minutes in FA buffer, then once for 10 minutes in FA buffer with 500mM NaCl, once for 5 minutes in FA buffer with 1M NaCl, once in for 10 minutes in TEL buffer (0.25M LiCl, 1% NP-40, 1% sodium deoxyholate, 1mM EDTA, 10mM Tris-HCl, pH 8.0), and twice for 5 minutes in TE pH 8.0. DNA was eluted twice by incubating beads with 50 µl elution buffer (TE containing 1% SDS and 250mM NaCl) at 65°C for 30 minutes each time. 10% of input DNA was also diluted in 100 µl elution buffer and processed in parallel with ChIP samples. Eluted DNA was treated with RNase A for 30 minutes at 37°C and then with 0.1 mg/ml Proteinase K for 1 hour at 50°C. Crosslinking was then reversed at 65°C overnight and DNA samples were purified using Qiagen PCR purification columns. Levels of ChIP DNA relative to inputs were then determined by RT-qPCR using the relative standard curve method of quantification. Primers used can be found in Supplemental Table S2.

Analysis of available RNA-seq and ChIP-seq datasets

RNA-seq and ChIP-seq data sets were published previously (Li et al., 2016) and accessed at Gene Expression Omnibus (GSE81523). For RNA-seq analysis, reads were aligned using the WS220/ce10 *C. elegans* genome assembly with TopHat2 (Kim et al., 2013). Default settings were used with the exception that the intron size was set to 10 – 22,000 bp (as appropriate for *C. elegans*). Expression analyses were performed using Cuffdiff (Trapnell et al., 2010) with quartile normalization. For ChIP-seq analysis, reads were aligned using the WS220/ce10 *C. elegans* genome assembly with Bowtie 1.1.2 (Langmead, 2010). ChIP-seq reads were mapped to promoters using Wormbase annotated transcription start sites. Due to the frequency with which many classical HSF-1 target genes are duplicated in the *C. elegans* genome, reads with two reportable alignments were retained to improve occupancy measure at these genes.

Fluorescence imaging and quantification of fluorescence intensity

Brightfield and fluorescence images of worms were acquired using a Zeiss AxioImager.Z2 microscope with a Hamamatsu camera and Zen software. Worms were immobilized on 3% agarose pads with 3 mM levamisole and imaged immediately. Fluorescence intensity was quantified in individual worms using FIJI (Schindelin et al., 2012). Regions of interest (areas in which the fluorescent protein is known to be expressed) were outlined within individual worms and fluorescence intensity normalized to area was determined for each worm. Background signal was then subtracted from all measurements to give the final fluorescence intensity per worm. Regions selected for quantification were: *hsp-16.2p::mcherry* – intestine; *hsp-4p::gfp* – intestine; *hsp-6p::gfp* – intestine; *cypA14p::gfp* – intestine; *daf-16p::daf-16::gfp* – entire animal.

Immunoprecipitation and western blotting

To perform immunoprecipitation, 20,000 – 30,000 day 3 adult worms were collected in M9 buffer and snap frozen. Worms pellets were then thawed and resuspended in co-IP lysis buffer (50 mM Tris-HCl pH 8, 120 mM NaCl, 0.5% NP-40, protease inhibitor cocktail (Roche)) and lysed by dounce homogenization on ice. For pulldowns, 2 mg of protein was combined with 20 µg of Protein-G Dynabeads and 5 µl of anti-Full length GFP (Clontech) in 1 ml total volume of co-IP buffer. Pulldowns were then incubated at 4°C overnight on a rotating wheel, following which, beads were washed 5 times in co-IP buffer and then re-suspended in 25 µl Laemmli buffer. Proteins were denatured by incubation at 95°C for 5 minutes and then subjected to SDS-PAGE and western blotting.

For western blotting, 40 µg of protein was separated by SDS-PAGE as per manufacturer's instructions) and transferred to a nitrocellulose membrane. Blots were then blocked for 1 hour at room temperature with 5% non-fat milk in PBS (w/v) and washed 3 times in PBS 0.2% Tween

(v/v). Blots were then incubated with primary antibodies for 1 hour at room temperature in PBS 0.02% Tween (anti-tubulin 1:10,000) or over-night at 4°C in 0.5% non-fat milk in PBS with 0.02% Tween (anti-GFP 1:1000, anti-LET-92 1:1000) and then washed three times for 10 minutes with PBS-0.2% Tween. Membranes were then incubated for 1 hour at room temperature with HRP conjugated secondary antibodies in PBS 0.02% Tween, washed three times for 15 minutes in PBS-0.2% Tween, and then exposed to ECL Plus (Amersham) as per manufacturer's instructions to develop signal. Blots were imaged using an ImageQuant gel imaging system (GE Healthcare). Brightness and contrast of blots was adjusted linearly across entire membranes to enhance visibility of bands. For phosphorylation analysis, Phos-tag reagent (Alpha laboratories) was added to SDS-PAGE gels as per manufacturer's instructions.

Stress resistance and lifespan assays

For thermo recovery assays, day 3 adult animals (40 – 50 per plate) were picked onto new seeded plates, wrapped tightly with parafilm, and submerged in a water bath at 35°C for 4 hours. Survival was then scored at 24 hour intervals following heat shock until the entire population was dead. Worms were scored as dead in the complete absence of touch response and pharyngeal pumping.

For lifespan analysis, experiments were performed at 20°C. Worms were allowed to reach adulthood and then scored for survival every other day throughout life. Animals were transferred to new plates every day for the first 7 days of adulthood to remove progeny and then transferred to new plates every 3 days thereafter. Worms were scored as dead in the absence of pharyngeal pumping and response to touch with a platinum pick.

Quantification of polyglutamine aggregation

Polyglutamine aggregation was scored manually using a Nikon SMZ stereo fluorescence dissection scope. Scorers were blinded to treatment groups and the number of aggregates was scored at each day until day 6 of adulthood (AM140) or until all worms exhibited at least one aggregate (AM738). Worms were transferred every day to remove progeny. Individual curves were then used to calculate the time taken, in days, for the population to reach 50% aggregation (Agg50 value).

Paralysis assay for assessment of proteotoxicity

To assess paralysis with age, animals were scored as paralysed if they failed to move > 1 body length in response to plate tap or gentle prodding with platinum wire. Paralysed worms were removed from plates and worms were scored every day until all worms were paralyzed. Progeny were removed by transferring adults to new plates every day.

Quantification and Statistical analysis

Statistical significance was calculated by Log-rank (Mantel-Cox) test for lifespan and stress resistance assays. One-way ANOVA with Tukey post analysis pair wise comparison of groups, two-way ANOVA with Bonferroni post analysis correction, or two-tailed Student's *t*-test were used for all other comparisons as stated in figure legends. All error bars represent SEM. The statistical tests used are declared in all figure legends and were calculated using GraphPad Prism (ANOVA, Log-rank) or Microsoft Excel (*t*-test). A minimum of 15 biological replicates were used for quantification of fluorescence images and between 72 and 168 worms were used per treatment group, per trial, for all lifespan assays, with 3 independent trials performed. At least 4 biological replicates were used for all other experiments except Figure 5E, where 3 biological replicates were used.

Supplemental Tables

Table S1: Sample numbers and statistics for survival curves (Related to Figures 2, 4 and 6, and supplemental Figures 2 and 6)

Table S2: List of primers used in this study (Related to STAR methods section: "*RNA extraction, cDNA synthesis and gene expression analyses"*)

Table S3: Effect of RNAi clones used in screen (Related to Figure 3)

References

Ahn, J.H., McAvoy, T., Rakhilin, S.V., Nishi, A., Greengard, P., and Nairn, A.C. (2007). Protein kinase A activates protein phosphatase 2A by phosphorylation of the B56delta subunit. Proc Natl Acad Sci U S A *104*, 2979-2984.

Alavez, S., Vantipalli, M.C., Zucker, D.J., Klang, I.M., and Lithgow, G.J. (2011). Amyloid-binding compounds maintain protein homeostasis during ageing and extend lifespan. Nature *472*, 226-229.

Asano, Y., Kawase, T., Okabe, A., Tsutsumi, S., Ichikawa, H., Tatebe, S., Kitabayashi, I., Tashiro, F., Namiki, H., Kondo, T., *et al.* (2016). IER5 generates a novel hypo-phosphorylated active form of HSF1 and contributes to tumorigenesis. Sci Rep *6*, 19174.

Ben-Zvi, A., Miller, E.A., and Morimoto, R.I. (2009). Collapse of proteostasis represents an early molecular event in Caenorhabditis elegans aging. Proc Natl Acad Sci U S A *106*, 14914-14919.

Bennett, C.F., Vander Wende, H., Simko, M., Klum, S., Barfield, S., Choi, H., Pineda, V.V., and Kaeberlein, M. (2014). Activation of the mitochondrial unfolded protein response does not predict longevity in Caenorhabditis elegans. Nat Commun *5*, 3483.

Boos, F., Kramer, L., Groh, C., Jung, F., Haberkant, P., Stein, F., Wollweber, F., Gackstatter, A., Zoller, E., van der Laan, M., *et al.* (2019). Mitochondrial protein-induced stress triggers a global adaptive transcriptional programme. Nat Cell Biol *21*, 442-451.

Borch Jensen, M., Qi, Y., Riley, R., Rabkina, L., and Jasper, H. (2017). PGAM5 promotes lasting FoxO activation after developmental mitochondrial stress and extends lifespan in Drosophila. Elife *6*.

Brenner, S. (1974). The genetics of Caenorhabditis elegans. Genetics *77*, 71-94.

Budzynski, M.A., Puustinen, M.C., Joutsen, J., and Sistonen, L. (2015). Uncoupling Stress-Inducible Phosphorylation of Heat Shock Factor 1 from Its Activation. Mol Cell Biol *35*, 2530-2540.

Dillin, A., Hsu, A.L., Arantes-Oliveira, N., Lehrer-Graiwer, J., Hsin, H., Fraser, A.G., Kamath, R.S., Ahringer, J., and Kenyon, C. (2002). Rates of behavior and aging specified by mitochondrial function during development. Science *298*, 2398-2401.

Gomez-Pastor, R., Burchfiel, E.T., and Thiele, D.J. (2018). Regulation of heat shock transcription factors and their roles in physiology and disease. Nat Rev Mol Cell Biol *19*, 4-19.

Govindan, J.A., Jayamani, E., Zhang, X., Mylonakis, E., and Ruvkun, G. (2015). Dialogue between E. coli free radical pathways and the mitochondria of C. elegans. Proc Natl Acad Sci U S A *112*, 12456-12461.

Haslbeck, M., Weinkauf, S., and Buchner, J. (2019). Small heat shock proteins: Simplicity meets complexity. J Biol Chem *294*, 2121-2132.

Hipp, M.S., Kasturi, P., and Hartl, F.U. (2019). The proteostasis network and its decline in ageing. Nat Rev Mol Cell Biol *20*, 421-435.

Hsu, A.L., Murphy, C.T., and Kenyon, C. (2003). Regulation of aging and age-related disease by DAF-16 and heat-shock factor. Science *300*, 1142-1145.

Kim, H.E., Grant, A.R., Simic, M.S., Kohnz, R.A., Nomura, D.K., Durieux, J., Riera, C.E., Sanchez, M., Kapernick, E., Wolff, S., *et al*. (2016). Lipid Biosynthesis Coordinates a Mitochondrial-to-Cytosolic Stress Response. Cell *166*, 1539-1552 e1516.

Kim, D., Pertea, G., Trapnell, C., Pimentel, H., Kelley, R., Salzberg, S.L. (2013). TopHat2: accurate alignment of transcriptomes in the presence of insertions, deletions and gene fusions. Genome biology *14*, R36.

Kinoshita, E., Kinoshita-Kikuta, E., and Koike, T. (2009). Separation and detection of large phosphoproteins using Phos-tag SDS-PAGE. Nat Protoc *4*, 1513-1521.

Labbadia, J., Brielmann, R.M., Neto, M.F., Lin, Y.F., Haynes, C.M., and Morimoto, R.I. (2017). Mitochondrial Stress Restores the Heat Shock Response and Prevents Proteostasis Collapse during Aging. Cell Rep *21*, 1481-1494.

Labbadia, J., and Morimoto, R.I. (2015a). The biology of proteostasis in aging and disease. Annu Rev Biochem *84*, 435-464.

Labbadia, J., and Morimoto, R.I. (2015b). Repression of the Heat Shock Response Is a Programmed Event at the Onset of Reproduction. Mol Cell *59*, 639-650.

Langmead, B. (2010). Aligning short sequencing reads with Bowtie. Current protocols in bioinformatics / editoral board, Andreas D Baxevanis [et al] Chapter 11: Unit 11 17.

Li, J., Chauve, L., Phelps, G., Brielmann, R.M., and Morimoto, R.I. (2016). E2F coregulates an essential HSF developmental program that is distinct from the heat-shock response. Genes Dev *30*, 2062-2075.

Liu, Y., Samuel, B.S., Breen, P.C., and Ruvkun, G. (2014). Caenorhabditis elegans pathways that surveil and defend mitochondria. Nature *508*, 406-410.

Livnat-Levanon, N., Kevei, E., Kleifeld, O., Krutauz, D., Segref, A., Rinaldi, T., Erpapazoglou, Z., Cohen, M., Reis, N., Hoppe, T., *et al.* (2014). Reversible 26S proteasome disassembly upon mitochondrial stress. Cell Rep *7*, 1371-1380.

Lopez-Otin, C., Blasco, M.A., Partridge, L., Serrano, M., and Kroemer, G. (2013). The hallmarks of aging. Cell *153*, 1194-1217.

Mao, K., Ji, F., Breen, P., Sewell, A., Han, M., Sadreyev, R., and Ruvkun, G. (2019). Mitochondrial Dysfunction in C. elegans Activates Mitochondrial Relocalization and Nuclear Hormone Receptor-Dependent Detoxification Genes. Cell Metab *29*, 1182-1191 e1184.

Matilainen, O., Sleiman, M.S.B., Quiros, P.M., Garcia, S., and Auwerx, J. (2017). The chromatin remodeling factor ISW-1 integrates organismal responses against nuclear and mitochondrial stress. Nat Commun *8*, 1818.

Morley, J.F., Brignull, H.R., Weyers, J.J., and Morimoto, R.I. (2002). The threshold for polyglutamine-expansion protein aggregation and cellular toxicity is dynamic and influenced by aging in Caenorhabditis elegans. Proc Natl Acad Sci U S A *99*, 10417-10422.

Morley, J.F., and Morimoto, R.I. (2004). Regulation of longevity in Caenorhabditis elegans by heat shock factor and molecular chaperones. Mol Biol Cell *15*, 657-664.

Munkacsy, E., Khan, M.H., Lane, R.K., Borror, M.B., Park, J.H., Bokov, A.F., Fisher, A.L., Link, C.D., and Rea, S.L. (2016). DLK-1, SEK-3 and PMK-3 Are Required for the Life Extension Induced by Mitochondrial Bioenergetic Disruption in C. elegans. PLoS Genet *12*, e1006133.

Ooi, F.K., and Prahlad, V. (2017). Olfactory experience primes the heat shock transcription factor HSF-1 to enhance the expression of molecular chaperones in C. elegans. Sci Signal *10*.

Prahlad, V., and Morimoto, R.I. (2011). Neuronal circuitry regulates the response of Caenorhabditis elegans to misfolded proteins. Proc Natl Acad Sci U S A *108*, 14204-14209.

Raman, D., and Pervaiz, S. (2019). Redox inhibition of protein phosphatase PP2A: Potential implications in oncogenesis and its progression. Redox Biol *27*, 101105.

Rea, S.L., Ventura, N., and Johnson, T.E. (2007). Relationship between mitochondrial electron transport chain dysfunction, development, and life extension in Caenorhabditis elegans. PLoS Biol *5*, e259.

Schiavi, A., Maglioni, S., Palikaras, K., Shaik, A., Strappazzon, F., Brinkmann, V., Torgovnick, A., Castelein, N., De Henau, S., Braeckman, B.P., *et al.* (2015). Iron-Starvation-Induced Mitophagy Mediates Lifespan Extension upon Mitochondrial Stress in C. elegans. Curr Biol *25*, 1810-1822.

Schindelin, J., Arganda-Carreras, I., Frise, E., Kaynig, V., Longair, M., Pietzsch, T., Preibisch, S., Rueden, C., Saalfeld, S., Schmid, B., *et al.* (2012). Fiji: an open-source platform for biological-image analysis. Nat Methods *9*, 676-682.

Segref, A., Kevei, E., Pokrzywa, W., Schmeisser, K., Mansfeld, J., Livnat-Levanon, N., Ensenauer, R., Glickman, M.H., Ristow, M., and Hoppe, T. (2014). Pathogenesis of human mitochondrial diseases is modulated by reduced activity of the ubiquitin/proteasome system. Cell Metab *19*, 642-652.

Shemesh, N., Shai, N., and Ben-Zvi, A. (2013). Germline stem cell arrest inhibits the collapse of somatic proteostasis early in Caenorhabditis elegans adulthood. Aging Cell *12*, 814-822.

Shore, D.E., Carr, C.E., and Ruvkun, G. (2012). Induction of cytoprotective pathways is central to the extension of lifespan conferred by multiple longevity pathways. PLoS Genet *8*, e1002792.

Sorrentino, V., Romani, M., Mouchiroud, L., Beck, J.S., Zhang, H., D'Amico, D., Moullan, N., Potenza, F., Schmid, A.W., Rietsch, S., *et al.* (2017). Enhancing mitochondrial proteostasis reduces amyloid-beta proteotoxicity. Nature *552*, 187-193.

Su, K.H., Dai, S., Tang, Z., Xu, M., and Dai, C. (2019). Heat Shock Factor 1 Is a Direct Antagonist of AMP-Activated Protein Kinase. Mol Cell *76*, 546-561 e548.

Sun, N., Youle, R.J., and Finkel, T. (2016). The Mitochondrial Basis of Aging. Mol Cell *61*, 654-666.

Trapnell, C., Williams, B.A., Pertea, G., Mortazavi, A., Kwan, G., van Baren, M.J., Salzberg, S.L., Wold, B.J., Pachter, L. (2010). Transcript assembly and quantification by RNA-Seq reveals unannotated transcripts and isoform switching during cell differentiation. Nature biotechnology *28*, 511-515

Tsang, W.Y., and Lemire, B.D. (2002). Mitochondrial genome content is regulated during nematode development. Biochem Biophys Res Commun *291*, 8-16.

Vos, M.J., Carra, S., Kanon, B., Bosveld, F., Klauke, K., Sibon, O.C., and Kampinga, H.H. (2016). Specific protein homeostatic functions of small heat-shock proteins increase lifespan. Aging Cell *15*, 217-226.

Vos, M.J., Zijlstra, M.P., Kanon, B., van Waarde-Verhagen, M.A., Brunt, E.R., Oosterveld-Hut, H.M., Carra, S., Sibon, O.C., and Kampinga, H.H. (2010). HSPB7 is the most potent polyQ aggregation suppressor within the HSPB family of molecular chaperones. Hum Mol Genet *19*, 4677-4693.

Walther, D.M., Kasturi, P., Zheng, M., Pinkert, S., Vecchi, G., Ciryam, P., Morimoto, R.I., Dobson, C.M., Vendruscolo, M., Mann, M., *et al.* (2015). Widespread Proteome Remodeling and Aggregation in Aging C. elegans. Cell *161*, 919-932.

Wang, X., and Chen, X.J. (2015). A cytosolic network suppressing mitochondria-mediated proteostatic stress and cell death. Nature *524*, 481-484.

Wrobel, L., Topf, U., Bragoszewski, P., Wiese, S., Sztolsztener, M.E., Oeljeklaus, S., Varabyova, A., Lirski, M., Chroscicki, P., Mroczek, S., *et al.* (2015). Mistargeted mitochondrial proteins activate a proteostatic response in the cytosol. Nature *524*, 485-488.

Wu, Z., Senchuk, M.M., Dues, D.J., Johnson, B.K., Cooper, J.F., Lew, L., Machiela, E., Schaar, C.E., DeJonge, H., Blackwell, T.K., *et al.* (2018). Mitochondrial unfolded protein response transcription factor ATFS-1 promotes longevity in a long-lived mitochondrial mutant through activation of stress response pathways. BMC Biol *16*, 147.

Yang, W., Wang, X., Liu, J., Duan, C., Gao, G., Lu, L., Yu, S., and Yang, H. (2018). PINK1 suppresses alpha-synuclein-induced neuronal injury: a novel mechanism in protein phosphatase 2A activation. Oncotarget *9*, 37-53.

Figure 1

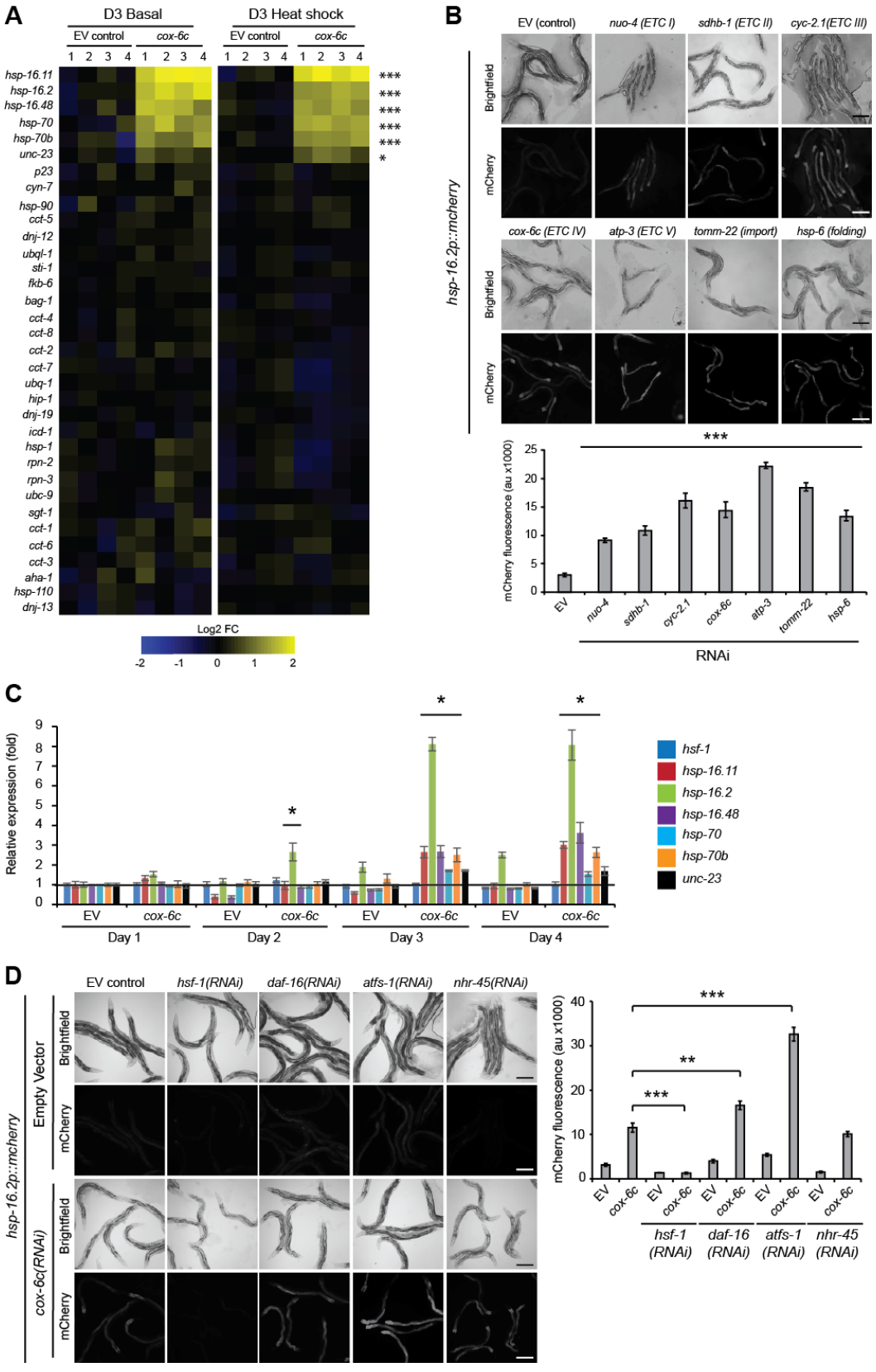
A
D3 Basal
D3 Heat shock
EV control
cox-6c
hsp-16.11
hsp-16.2
hsp-16.48
hsp-70
hsp-70b
unc-23
p23
cyn-7
hsp-90
cct-5
dnj-12
ubql-1
sti-1
fkb-6
bag-1
cct-4
cct-8
cct-2
cct-7
ubq-1
hip-1
dnj-19
icd-1
hsp-1
rpn-2
rpn-3
ubc-9
sgt-1
cct-1
cct-6
cct-3
aha-1
hsp-110
dnj-13
Log2 FC
B
EV (control)
nuo-4 (ETC I)
sdhb-1 (ETC II)
cyc-2.1(ETC III)
cox-6c (ETC IV)
atp-3 (ETC V)
tomm-22 (import)
hsp-6 (folding)
Brightfield
mCherry
hsp-16.2p::mcherry
mCherry fluorescence (au x1000)
RNAi
C
Relative expression (fold)
Day 1
Day 2
Day 3
Day 4
hsf-1
D
EV control
hsf-1(RNAi)
daf-16(RNAi)
atfs-1(RNAi)
nhr-45(RNAi)
Empty Vector
cox-6c(RNAi)

Figure 2

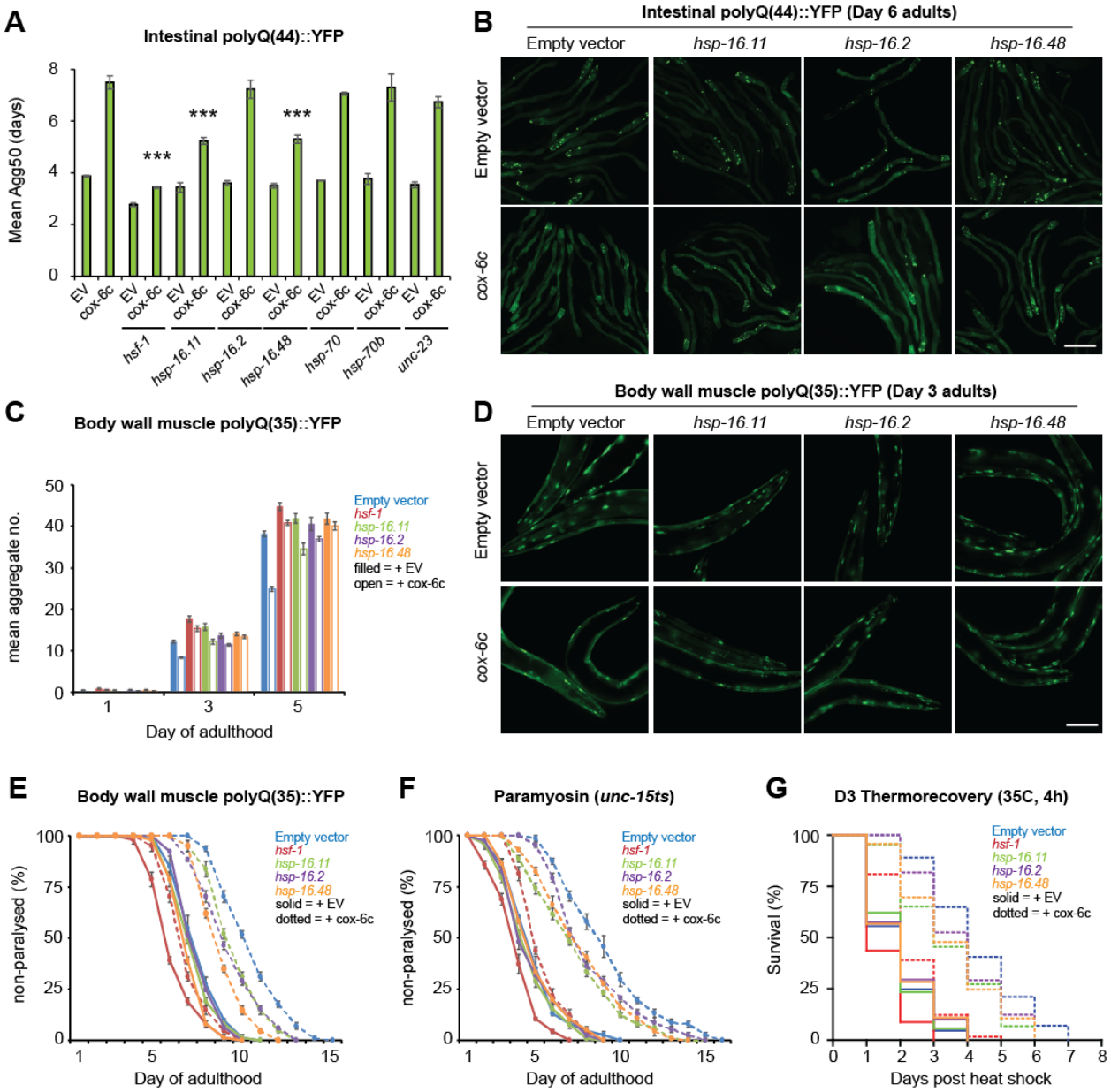
A
Intestinal polyQ(44)::YFP
Mean Agg50 (days)
***
***
***
EV
cox-6c
hsf-1
hsp-16.11
hsp-16.2
hsp-16.48
hsp-70
hsp-70b
unc-23
B
Intestinal polyQ(44)::YFP (Day 6 adults)
Empty vector
hsp-16.11
hsp-16.2
hsp-16.48
Empty vector
cox-6c
C
Body wall muscle polyQ(35)::YFP
mean aggregate no.
Day of adulthood
Empty vector
hsf-1
hsp-16.11
hsp-16.2
hsp-16.48
filled = + EV
open = + cox-6c
D
Body wall muscle polyQ(35)::YFP (Day 3 adults)
Empty vector
hsp-16.11
hsp-16.2
hsp-16.48
Empty vector
cox-6c
E
Body wall muscle polyQ(35)::YFP
non-paralysed (%)
Day of adulthood
Empty vector
hsf-1
hsp-16.11
hsp-16.2
hsp-16.48
solid = + EV
dotted = + cox-6c
F
Paramyosin (unc-15ts)
non-paralysed (%)
Day of adulthood
Empty vector
hsf-1
hsp-16.11
hsp-16.2
hsp-16.48
solid = + EV
dotted = + cox-6c
G
D3 Thermorecovery (35C, 4h)
Survival (%)
Days post heat shock
Empty vector
hsf-1
hsp-16.11
hsp-16.2
hsp-16.48
solid = + EV
dotted = + cox-6c

Figure 3

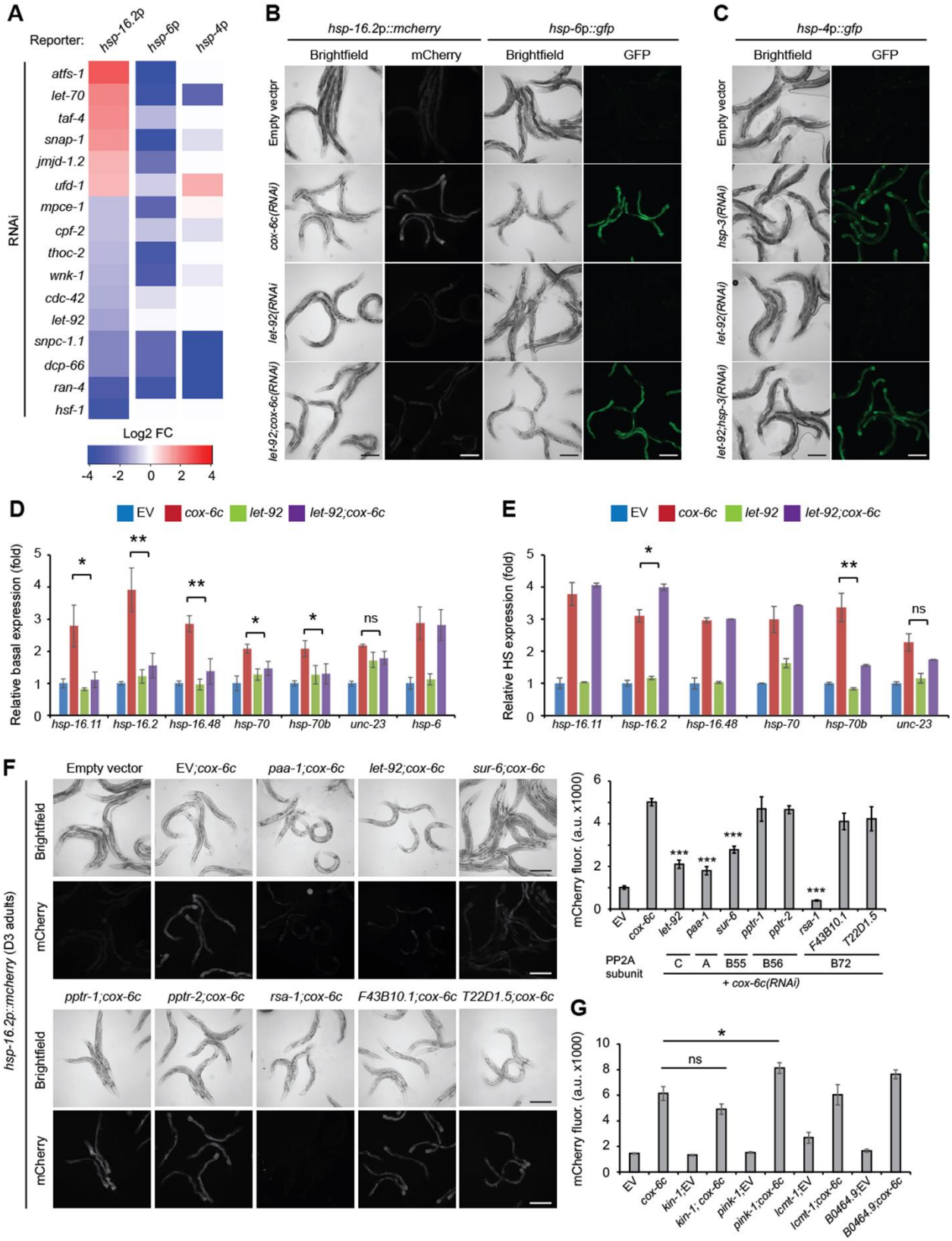
A
Reporter:
hsp-16.2p
hsp-6p
hsp-4p
RNAi
atfs-1
let-70
taf-4
snap-1
jmjd-1.2
ufd-1
mpce-1
cpf-2
thoc-2
wnk-1
cdc-42
let-92
snpc-1.1
dcp-66
ran-4
hsf-1
Log2 FC
-4 -2 0 2 4
B
hsp-16.2p::mcherry
hsp-6p::gfp
Brightfield
mCherry
Brightfield
GFP
Empty vectpr
cox-6c(RNAi)
let-92(RNAi
let-92;cox-6c(RNAi)
C
hsp-4p::gfp
Brightfield
GFP
Empty vector
hsp-3(RNAi)
let-92(RNAi)
let-92;hsp-3(RNAi)
D
EV
cox-6c
let-92
let-92;cox-6c
Relative basal expression (fold)
hsp-16.11
hsp-16.2
hsp-16.48
hsp-70
hsp-70b
unc-23
hsp-6
E
EV
cox-6c
let-92
let-92;cox-6c
Relative HS expression (fold)
hsp-16.11
hsp-16.2
hsp-16.48
hsp-70
hsp-70b
unc-23
F
hsp-16.2p::mcherry (D3 adults)
Empty vector
EV;cox-6c
paa-1;cox-6c
let-92;cox-6c
sur-6;cox-6c
Brightfield
mCherry
pptr-1;cox-6c
pptr-2;cox-6c
rsa-1;cox-6c
F43B10.1;cox-6c
T22D1.5;cox-6c
mCherry fluor. (a.u. x1000)
EV
cox-6c
let-92
paa-1
sur-6
pptr-1
pptr-2
rsa-1
F43B10.1
T22D1.5
PP2A subunit
C
A
B55
B56
B72
+ cox-6c(RNAi)
G
mCherry fluor. (a.u. x1000)
ns
EV
cox-6c
kin-1;EV
kin-1; cox-6c
pink-1;EV
pink-1;cox-6c
lcmt-1;EV
lcmt-1;cox-6c
B0464.9;EV
B0464.9;cox-6c

Figure 4

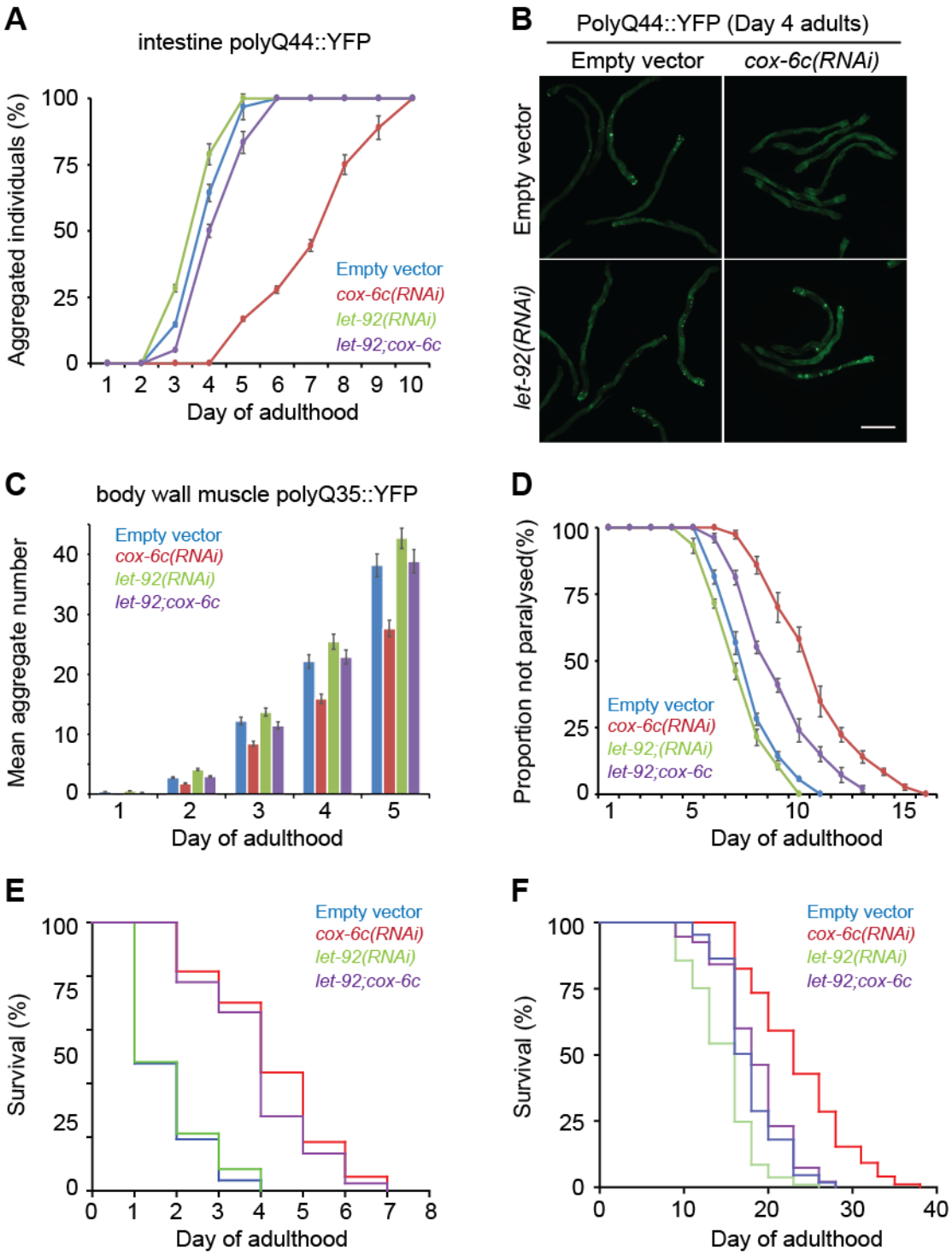
A
intestine polyQ44::YFP
Aggregated individuals (%)
Day of adulthood
Empty vector
cox-6c(RNAi)
let-92(RNAi)
let-92;cox-6c
B
PolyQ44::YFP (Day 4 adults)
Empty vector
cox-6c(RNAi)
Empty vector
let-92(RNAi)
C
body wall muscle polyQ35::YFP
Mean aggregate number
Day of adulthood
D
Proportion not paralysed(%)
Day of adulthood
E
Survival (%)
Day of adulthood
F
Survival (%)
Day of adulthood

Figure 5

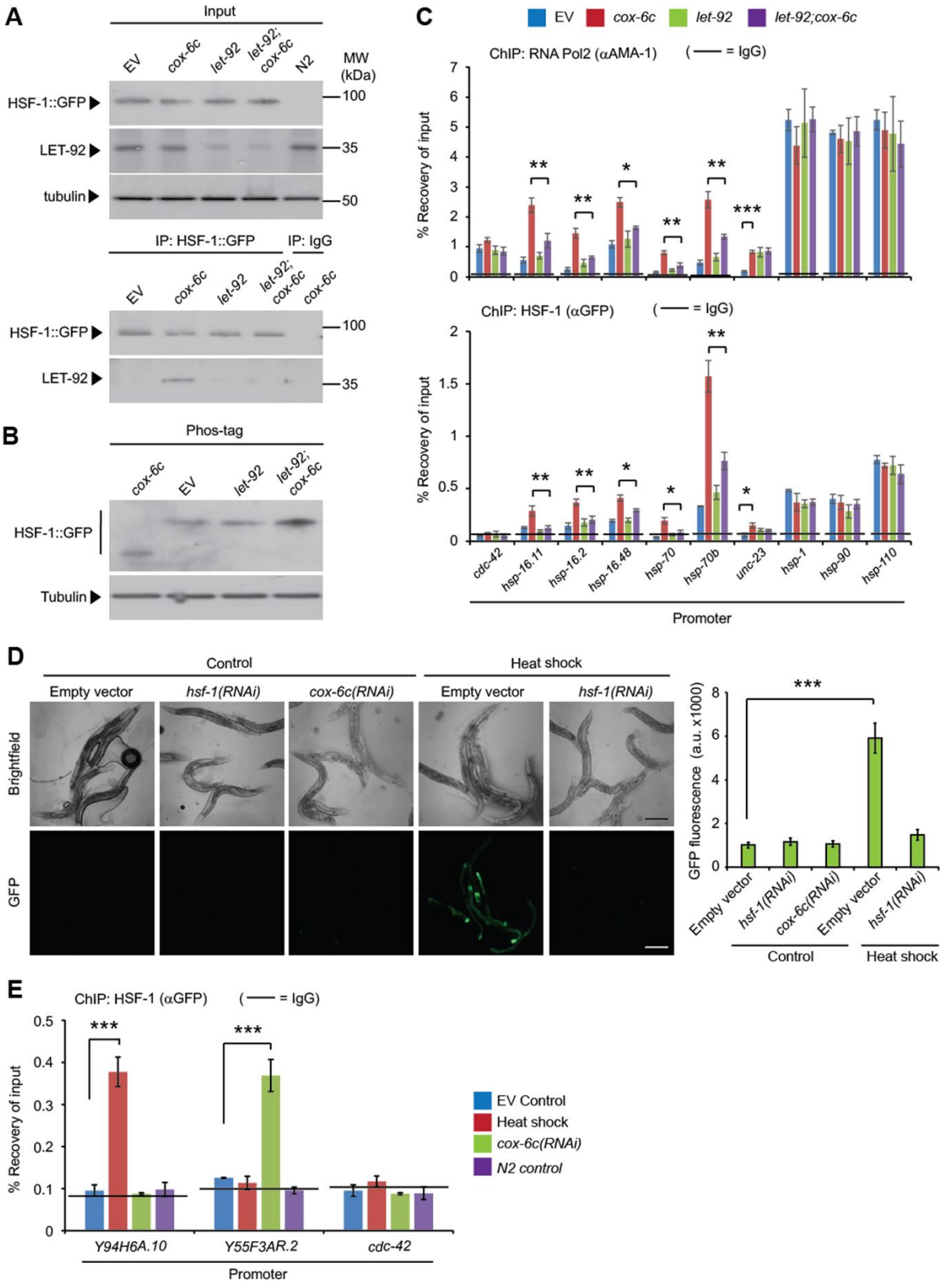
A
Input
EV
cox-6c
let-92
let-92; cox-6c
N2
MW (kDa)
HSF-1::GFP
LET-92
tubulin
100
35
50
IP: HSF-1::GFP
IP: IgG
cox-6c
B
Phos-tag
Tubulin
C
EV
cox-6c
let-92
let-92;cox-6c
ChIP: RNA Pol2 (αAMA-1)
(—— = IgG)
% Recovery of input
ChIP: HSF-1 (αGFP)
cdc-42
hsp-16.11
hsp-16.2
hsp-16.48
hsp-70
hsp-70b
unc-23
hsp-1
hsp-90
hsp-110
Promoter
D
Control
Heat shock
Empty vector
hsf-1(RNAi)
cox-6c(RNAi)
Brightfield
GFP
GFP fluorescence (a.u. x1000)
E
ChIP: HSF-1 (αGFP)
(—— = IgG)
% Recovery of input
Y94H6A.10
Y55F3AR.2
cdc-42
Promoter
EV Control
Heat shock
cox-6c(RNAi)
N2 control

Figure 6

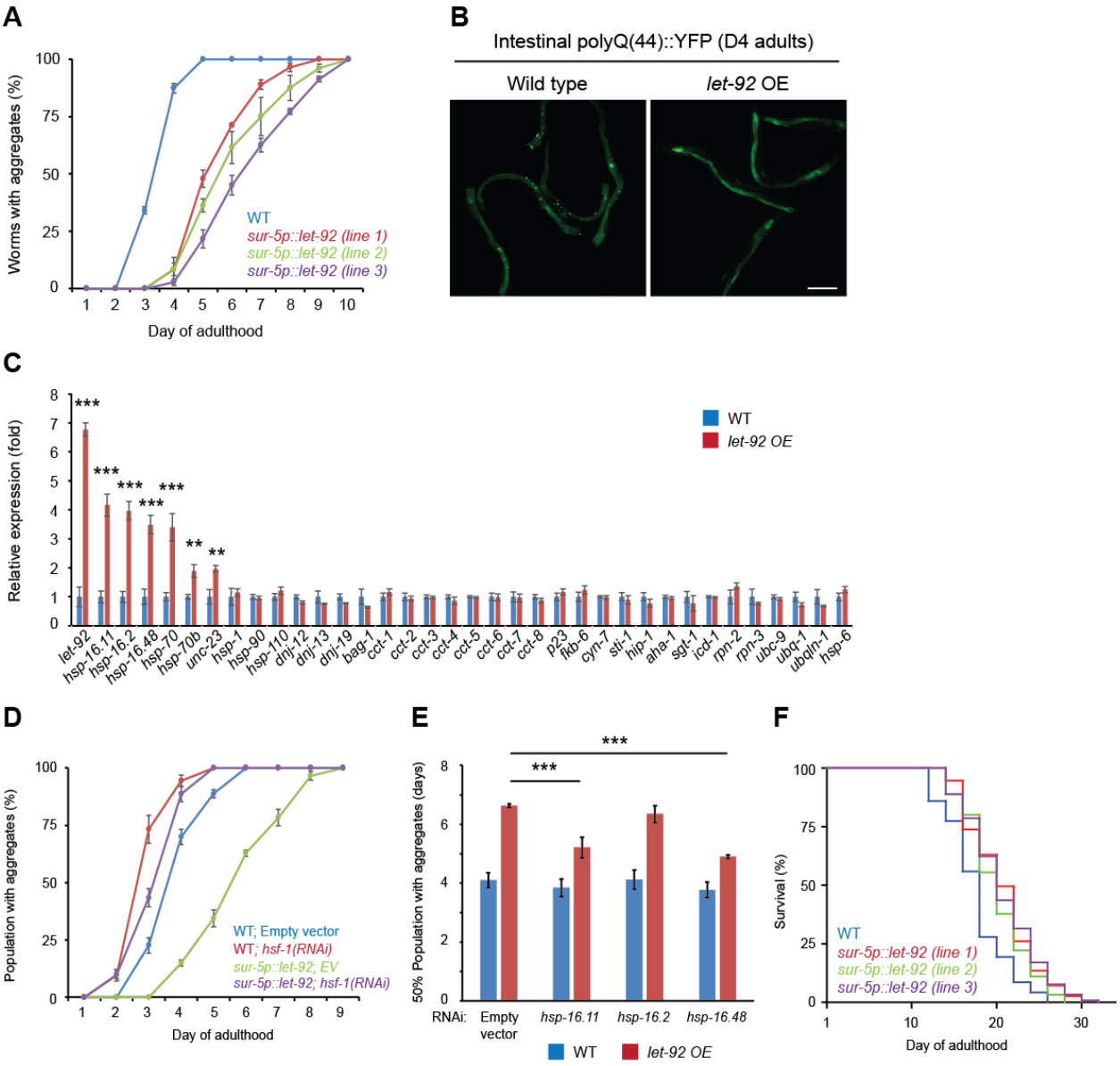
A
Worms with aggregates (%)
Day of adulthood
WT
sur-5p::let-92 (line 1)
sur-5p::let-92 (line 2)
sur-5p::let-92 (line 3)
B
Intestinal polyQ(44)::YFP (D4 adults)
Wild type
let-92 OE
C
Relative expression (fold)
WT
let-92 OE
let-92
hsp-16.11
hsp-16.2
hsp-16.48
hsp-70
hsp-70b
unc-23
hsp-1
hsp-90
hsp-110
dnj-12
dnj-13
dnj-19
bag-1
cct-1
cct-2
cct-3
cct-4
cct-5
cct-6
cct-7
cct-8
p23
fkb-6
cyn-7
sti-1
hip-1
aha-1
sgt-1
icd-1
rpn-2
rpn-3
ubc-9
ubq-1
ubqln-1
hsp-6
D
Population with aggregates (%)
Day of adulthood
WT; Empty vector
WT; hsf-1(RNAi)
sur-5p::let-92; EV
sur-5p::let-92; hsf-1(RNAi)
E
50% Population with aggregates (days)
RNAi:
Empty vector
hsp-16.11
hsp-16.2
hsp-16.48
WT
let-92 OE
F
Survival (%)
Day of adulthood
WT
sur-5p::let-92 (line 1)
sur-5p::let-92 (line 2)
sur-5p::let-92 (line 3)

Figure 7

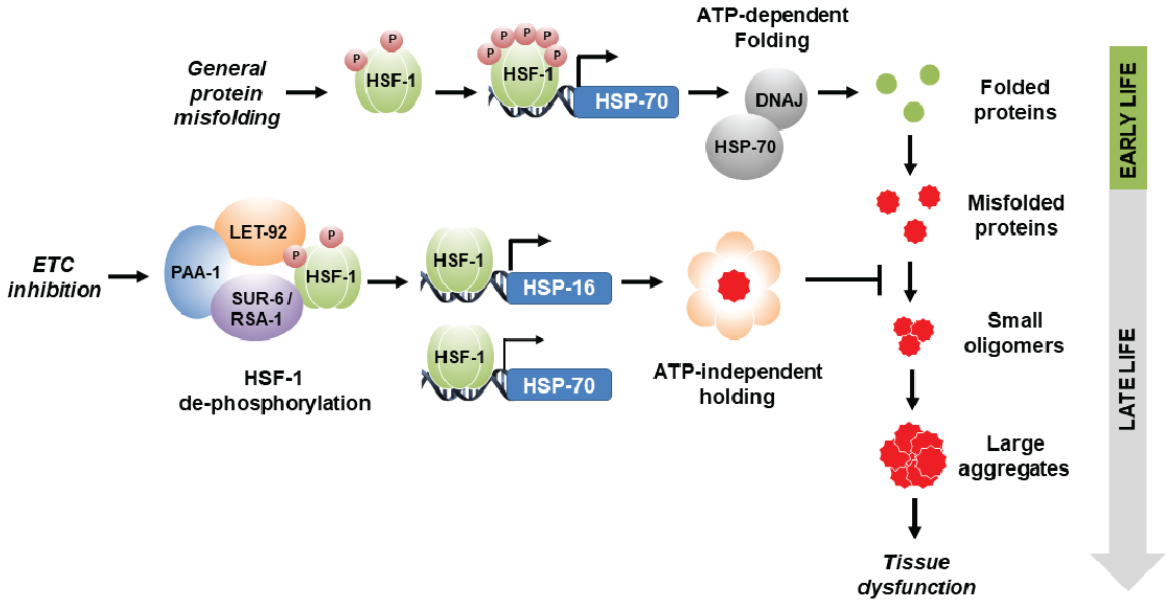
General protein misfolding
HSF-1
HSF-1
HSP-70
ATP-dependent Folding
DNAJ
HSP-70
Folded proteins
Misfolded proteins
Small oligomers
Large aggregates
Tissue dysfunction
EARLY LIFE
LATE LIFE
ETC inhibition
LET-92
PAA-1
SUR-6 / RSA-1
HSF-1
HSF-1 de-phosphorylation
HSF-1
HSP-16
HSF-1
HSP-70
ATP-independent holding